석사 학위논문
Master's Thesis

3차원 부유체에 대한 유탄성 해석

Hydroelastic analysis of three dimensional floating structures

김 기 태 (金 基 泰 Kim, Ki-Tae)
기계항공시스템학부, 해양시스템공학전공
School of Mechanical, Aerospace and Systems Engineering
Department of Ocean Systems Engineering

KAIST

2011

3차원 부유체에 대한 유탄성 해석

Hydroelastic analysis of three dimensional floating structures

Hydroelastic analysis of three dimensional floating structures

Advisor : Professor Lee, Phill-Seung

by

Kim, Ki-Tae

School of Mechanical, Aerospace and Systems Engineering

Department of Ocean Systems Engineering

KAIST

A thesis submitted to the faculty of KAIST in partial fulfillment of the requirements for the degree of Master of Science in Engineering in the School of Mechanical, Aerospace and Systems Engineering, Department of Ocean Systems Engineering . The study was conducted in accordance with Code of Research Ethics[1].

2002. 12. 5.

Approved by

Professor Lee, Phill-Seung

[Advisor]

[1]Declaration of Ethical Conduct in Research: I, as a graduate student of KAIST, hereby declare that I have not committed any acts that may damage the credibility of my research. These include, but are not limited to: falsification, thesis written by someone else, distortion of research findings or plagiarism. I affirm that my thesis contains honest conclusions based on my own careful research under the guidance of my thesis advisor.

3차원 부유체에 대한 유탄성 해석

김 기 태

위 논문은 한국과학기술원 석사학위논문으로
학위논문심사위원회에서 심사 통과하였음.

2011년 05월 23일

심사위원장 이 필 승 (인)

심사위원 박 광 춘 (인)

심사위원 최 우 영 (인)

심사위원 홍 도 천 (인)

MOSE
20094123

김 기 태. Kim, Ki-Tae. Hydroelastic analysis of three dimensional floating structures. 3차원 부유체에 대한 유탄성 해석. School of Mechanical, Aerospace and Systems Engineering, Department of Ocean Systems Engineering . 2011. 59p. Advisor Prof. Lee, Phill-Seung. Text in English.

ABSTRACT

In this study, we analyze floating structures under regular (time-harmonic) surface water waves. Under the appropriate assumptions, the coupled equations that represent three dimensional hydroelastic behavior of the structures are derived. The structural domain is modeled by shell finite elements, and the fluid-structure interface boundary surface is also discretized to solve the coupled equations. To validate our mathematical formulation, we compare the representative results with the experiment results for a mat-like floating structure, and the quite satisfactory results are produced. We also carry out additional two models, a box-like floating structure and a Wigley hull, for three dimensional aspects of hydroelasticity, and get the reasonable results.

Contents

List of Tables

List of Figures

Chapter 1. Introduction

Typically the dynamics of a floating structure has been based on the assumption of rigid motion, because it could produce acceptable results with more simple and efficient analysis. But as the size of ships and offshore structures is getting larger, the elasticity of the floating structure becomes dominant, so this assumption could not support the analysis any longer. Hydroelastic analysis which considers the effect of the structure's elasticity in wave-structure interaction problems has attracted considerable interests in the last ten years and developed well recently. The representative example of this study is the analysis of a mat-like very large floating structures such as a floating air port, a pontoon-type bridge, large floating offshore structures, ice floes, and so on. Kashiwagi M. [7] and Watanabe E. *et al.* [20] presented reviews of these works. In these works, the floating structure is modeled as a thin large plate or beam and the potential fluid is adopted. The motions of the structure and the amplitude of the incident wave are assumed small, and the most of the analysis was carried out in the frequency domain. The commonly used solving technique for these seakeeping problems are the modal expansion method and the direct method. To determine the motion of the structure, the modal expansion method use a sum of modal functions such as products of free-free beam modes, B-spline functions, the modes of vibrations of a free plate, and so on. In the direct method, the motion of the equation is directly solved without the modal functions.

The classical approach for the fluid problem in wave-structure interaction analysis decomposes the fluid velocity potential into diffraction and radiation potential, and this procedure extended to hydroelastic analysis by Bishop and Price [4]. The other approach just couples the motion of the structure and the fluid pressure which relates to the fluid velocity potential without separating the problem into diffraction and radiation components. Most of the recent hydroelastic analysis of floating structures have used the second approach, and representative works have been done by Khabakhpasheva T.I. and Korobkin, A.A. [8] ; Taylor R.E. [18] where they solved the whole equations by using the Galerkin method.

The hydroelastic studies performed up to recently are mainly for the beam structures or plate structures. There are, however, many different shape of structures in the ocean environment. It is evident that there are limitations in modeling the ships and the offshore structures as beam or plate structures. To extend the hydroelastic analysis into these various shape of structures, we studied a hydroelastic behavior of floating structures in three dimensional case. We modeled the floating structure as shell structure, because most of the ships or the offshore structures are thinner in one direction than in the other directions. The potential fluid was adopted and we didn't separate it. Overall schema of the problems and assumptions we applied are described in chapter 2. In this chapter, we also derive a general coupled equations where the displacements of the structure and the fluid pressure are connected. Using this mathematical formulation, in chapter 3, we transform the coupled equation to a discrete linear system to solve it. Finally in chapter 4, we evaluate our mathematical formulation using a mat-like model and compare the results with an experiment data. To see the three dimensional aspects of the hydroelasticity, we also consider a box-like model and a Wigley hull. In the Wigley hull example, we compare our results with the other numerical results performed by Riggs H.R. *et al.* [15].

Chapter 2. General theory

This chapter describes the general procedure of physical and mathematical modeling of the problem. First we present the assumptions which are valid for this analysis, and then derive the governing equations where the structure equation and the fluid eqatuion are coupled each other. The final coupled equations are the variational forms for the finite and boundary element procedure which will be introduced next chapter.

2.1 Overall description and assumptions

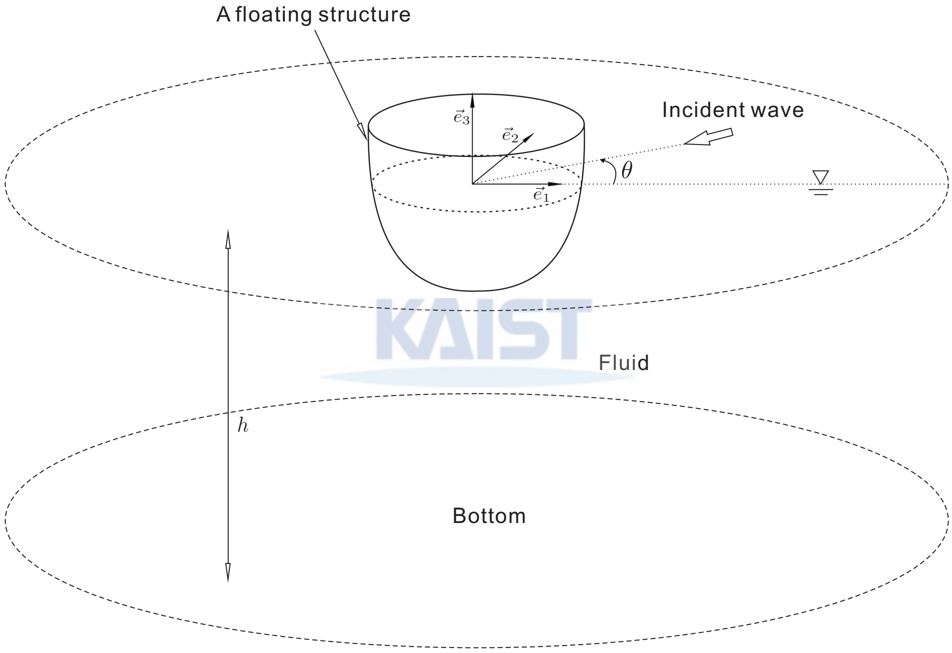

Figure 2.1: Overall schema of the problem

Fig. 2.1 represents an overall schema of the physical problem that we are going to analyze. A structure is floating on the water in a fixed Cartesian coordinate system, the origin of which is located on the centroid of the water plane area corresponded to a original configuration. The water depth is h, and a wave is coming with an incident angle θ. The incident angle θ is the angle between the x-axis and the incident wave, and positive value when it rotates counterclockwise.

We assume that the material is homogeneous, isotropic, and linear elastic. The displacements and strains are small, so all related computations can be performed over original reference frame. This assumption is also applied to the fluid, but in this case velocities and rate of strains are corresponded physical parameters. The fluid is assumed that it is Newtonian isotropic, incompressible, inviscid, and irrotational fluid. The incident wave is assumed that it is coming continuously with angular frequency ω, as a result the motion of the structure and the fluid are time harmonic with same frequency, if we assume that the system of that is linear. We assume also the amplitude of the wave is very small compared with the wave length. This make it possible that the free surface boundary condition can be linearized at $x_3 = 0$, which will be explained later.

2.2 Modeling of the floating structure

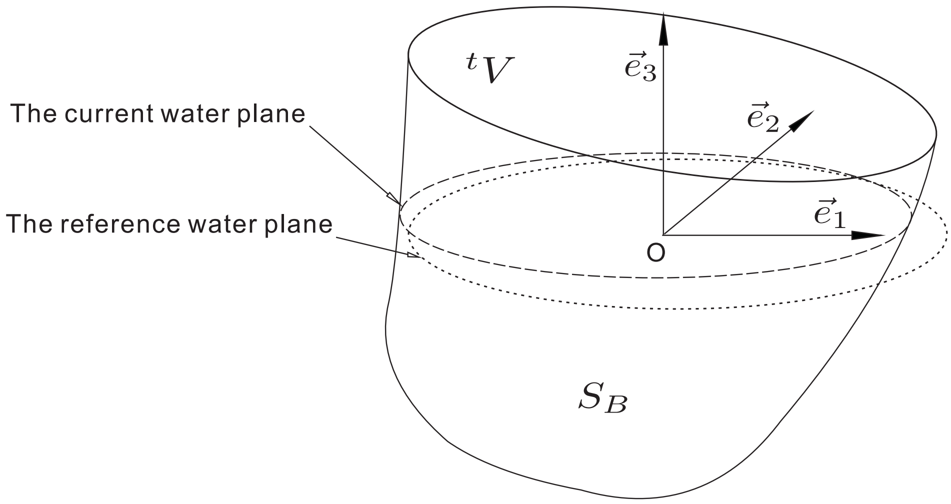

Figure 2.2: The floating structure in current state

Consider the equilibrium state of the floating structure as shown in Fig. 2.2. The reference means the original configuration of the structure. ^tV denotes the volume that the structure occupies currently and S_B the wet surface. The Cartesian coordinate system is fixed on the centroid of the reference water plane area, the point O. From now on, in this coordinate system we express some vector 'v' as $\mathbf{v}$ or $v_i\mathbf{e_i}$ or v_i and some matrix 'M' as $\mathbb{M}$ or M_{ij} where the indices i and j vary from 1 to 3 respectively, and we adopt Einstein summation convention. We define the vector $\mathbf{{}^0x}$ as a material point in the reference configuration, the vector $\mathbf{{}^tX}$ as a material point in the current configuration. So we can express a displacement vector $\mathbf{U}$ as $\mathbf{U} = \mathbf{{}^tX} - \mathbf{{}^0x}$ if $\mathbf{{}^0x}$ and $\mathbf{{}^tX}$ represent a same particle.

The balance law of linear momentum gives the following differential equation:

$$\frac{\partial \sigma'_{ij}}{\partial x_j} + \rho_s F_i - \rho_s \ddot{U}_i = 0 \qquad \text{in the structure domain} \tag{2.1}$$

where σ'_{ij} is Cauchy's stress tensor, ρ_s is the density of the structure, and F_i is the applied body force per unit mass. For simplicity, we introduce '$\ddot{\ }$' to represent the material time derivative, and we define $\sigma'_{ij} = \sigma_{ij}(\mathbf{x})\,T(t)$ and $\mathbf{U} = \mathbf{u}(\mathbf{{}^0x})\,T(t)$ where $T(t)$ is a arbitrary function of time and $\mathbf{x}$ is a spatial point. If we multiply (2.1) by the virtual displacements $\overline{u}_i$, integrate by parts, and apply the divergence theorem, we get

$$\int_{^tV} \rho_s \ddot{U}_i \bar{u}_i \,\mathrm{d}^tV + \int_{^tV} \sigma'_{ij} \frac{\partial \bar{u}_i}{\partial x_j} \,\mathrm{d}^tV = \int_{^tV} \rho_s F_i \bar{u}_i \,\mathrm{d}^tV + \int_{^tS} \sigma'_{ij} n_j \bar{u}_i \,\mathrm{d}^tS \tag{2.2}$$

where $\mathbf{n}$ denotes unit normal vectors outward from the structure domain, ^tS is the surface of the structure. From the symmetry of the stress tensor which comes from the balance law of angular momentum, we have

$$\sigma_{ij} \frac{\partial \bar{u}_i}{\partial x_j} = \sigma_{ij} \left(\frac{\partial \bar{u}_i}{\partial x_j} + \frac{\partial \bar{u}_j}{\partial x_i} \right) = \sigma_{ij} \bar{\epsilon}_{ij} \tag{2.3}$$

and therefore

$$\int_{^tV} \rho_s \ddot{U}_i \bar{u}_i \,\mathrm{d}^tV + \int_{^tV} \sigma'_{ij} \bar{\epsilon}_{ij} \,\mathrm{d}^tV = \int_{^tV} \rho_s F_i \bar{u}_i \,\mathrm{d}^tV + \int_{^tS} \sigma'_{ij} n_j \bar{u}_i \,\mathrm{d}^tS \tag{2.4}$$

where $\bar{\epsilon}_{ij}$ is the virtual strains.

(2.4) is the variational formulation for the structure part. The most important fact and the difference from the ordinary structural problem are that neither tractions nor displacements are specified on the wet surface. We just know that structure's tractions and velocities are same with fluid's on this surface. So we need another information that is related to the fluid.

2.2.1 Initial stress problem

Before the floating structure undergoes the incident wave, we have to find the displacements in the statically equilibrium state. We define this problem as 'Initial stress problem'. This problem is straightforward because on the wetted surface the traction distributions are replaced with a function of displacements. That is:

$$\mathbf{T} = -\begin{bmatrix} Pn_1 \\ Pn_2 \\ Pn_3 \end{bmatrix} \qquad \text{on the wet surface} \tag{2.5}$$

where $\mathbf{T}$ means the traction and P is the water pressure(Gauge pressure). In static fluid the pressure is nothing but $P = -\rho_w g x_3$ where ρ_w is the density of the fluid, and

$$\mathbf{F} = \begin{bmatrix} 0 \\ 0 \\ -g \end{bmatrix} \qquad \text{in } {}^tV \tag{2.6}$$

where g is the acceleration of gravity. So we obtain

$$\int_{^tV} \sigma_{ij}\bar{\epsilon}_{ij}\, \mathrm{d}^tV = -\int_{^tV} \rho_s g \bar{u}_3\, \mathrm{d}^tV + \int_{^tS_B} \rho_w({}^0x_3 + u_3) n_i \bar{u}_i\, \mathrm{d}^tS_B \tag{2.7}$$

If we introduce the following stress and engineering strain vector:

$$\begin{aligned} \boldsymbol{\sigma}^T &= [\,\sigma_{11}\ \sigma_{22}\ \sigma_{33}\ \sigma_{12}\ \sigma_{23}\ \sigma_{31}\,] \\ \boldsymbol{\epsilon}^T &= [\,\epsilon_{11}\ \epsilon_{22}\ \epsilon_{33}\ \gamma_{12}\ \gamma_{23}\ \gamma_{31}\,] \qquad \text{where} \quad \gamma_{ij} = \frac{\partial u_i}{\partial x_j} + \frac{\partial u_j}{\partial x_i} \end{aligned} \tag{2.8}$$

then we finally get

$$\int_{^tV} \bar{\boldsymbol{\epsilon}}^T \boldsymbol{\sigma}\, \mathrm{d}^tV = -\int_{^tV} \rho_s g \bar{u}_3\, \mathrm{d}^tV + \int_{^tS_B} \rho_w({}^0x_3 + u_3)\bar{\mathbf{u}}^T \mathbf{n}\, \mathrm{d}^tS_B \tag{2.9}$$

If the geometry of the structure is simple and the draft is very small, it doesn't need to compute (2.9) because we can easily find out the statically equilibrium state of it and the initial stress is negligibly small.

2.2.2 Steady state problem

The incident wave that the angular frequency is ω would excite the floating structure with same frequency. This is valid when the system is linear, and this means that the relation of input(ex. force) and output(ex. displacement) satisfies the linearity. We define the steady state such that time goes enough so that the initial conditions of the structure have no effects on it. This problem is a little difficult because as we mentioned before it requires one more equation related to the fluid.

Inserting (2.5) into (2.4) with linearized Bernoulli's equation $P = -\rho_w \frac{\partial \Phi}{\partial t} - \rho_w g x_3$ where Φ is the velocity potential (a scalar valued function) that we will explain later, then we have

$$\begin{aligned}\int_{{}^tV} \rho_s\, {}^s\ddot{U}_i \bar{u}_i \,\mathrm{d}^tV + \int_{{}^tV} ({}^i\sigma_{ij} +{}^s \sigma'_{ij})\bar{\epsilon}_{ij} \,\mathrm{d}^tV &= -\int_{{}^tV} \rho_s g \bar{u}_3 \,\mathrm{d}^tV + \int_{{}^tS_B} \rho_w \frac{\partial \Phi}{\partial t} n_i \bar{u}_i \,\mathrm{d}^tS_B \\ &\quad + \int_{{}^tS_B} \rho_w g ({}^0x_3 +{}^i u_3 +{}^s U_3) n_i \bar{u}_i \,\mathrm{d}^tS_B \end{aligned} \quad (2.10)$$

where the left superscript i and s mean 'Initial stress problem' and 'Steady state problem' respectively. Because of (2.7) or (2.9), (2.10) becomes

$$\int_{{}^tV} \rho_s \ddot{U}_i \bar{u}_i \,\mathrm{d}^tV + \int_{{}^tV} \sigma'_{ij}\bar{\epsilon}_{ij} \,\mathrm{d}^tV = \int_{{}^tS_B} \rho_w \frac{\partial \Phi}{\partial t} n_i \bar{u}_i \,\mathrm{d}^tS_B + \int_{{}^tS_B} \rho_w g U_3 n_i \bar{u}_i \,\mathrm{d}^tS_B \quad (2.11)$$

or

$$\int_{{}^tV} \rho_s \bar{\mathbf{u}}^T \frac{D^2\mathbf{U}}{Dt^2} \,\mathrm{d}^tV + \int_{{}^tV} \bar{\boldsymbol{\epsilon}}^T \boldsymbol{\sigma}' \,\mathrm{d}^tV = \int_{{}^tS_B} \rho_w \frac{\partial \Phi}{\partial t} \bar{\mathbf{u}}^T \mathbf{n} \,\mathrm{d}^tS_B + \int_{{}^tS_B} \rho_w g U_3 \bar{\mathbf{u}}^T \mathbf{n} \,\mathrm{d}^tS_B \quad (2.12)$$

As you can easily find in the above equation, the unknown variables that we have to find are the displacements vector function $\mathbf{u}$ and the velocity potential function Φ. To solve this variational equation, we need to derive the variational formulation for the fluid.

Finally if we assume that $T(t) = e^{i\omega t}$, that is:

$$\begin{aligned} \Phi &= \phi(\mathbf{x}) e^{i\omega t} \\ \sigma'_{ij} &= \sigma_{ij}(\mathbf{x}) e^{i\omega t} \\ \mathbf{U} &= \mathbf{u}({}^0\mathbf{x}) e^{i\omega t} \end{aligned} \quad (2.13)$$

then we obtain

$$-\int_{{}^tV} \omega^2 \rho_s \bar{\mathbf{u}}^T \mathbf{u} \,\mathrm{d}^tV + \int_{{}^tV} \bar{\boldsymbol{\epsilon}}^T \boldsymbol{\sigma} \,\mathrm{d}^tV = \int_{{}^tS_B} i\omega\rho_w \phi \bar{\mathbf{u}}^T \mathbf{n} \,\mathrm{d}^tS_B + \int_{{}^tS_B} \rho_w g u_3 \bar{\mathbf{u}}^T \mathbf{n} \,\mathrm{d}^tS_B \quad (2.14)$$

As you can see in the final equation of motion for the structure, (2.14), the velocity potential of the fluid is included. This velocity potential comes from linearized Bernoulli's equation and has to do with the external fluid pressure.

2.3 Modeling of the fluid

With the continuity equation which comes from the mass conservation, the assumption of incompressible fluid, and the assumption of irrotational fluid, we start Laplace's equation for the velocity potential:

$$\nabla^2 \Phi = 0 \qquad \text{in the fluid domain} \tag{2.15}$$

From the linear momentum conservation with the above assumptions and additional assumptions of Newtonian, isotropic, and inviscid fluid, we can derive Bernoulli's equation for the potential fluid:

$$\frac{\partial \Phi}{\partial t} + \frac{1}{2}\nabla\Phi \cdot \nabla\Phi + \frac{P}{\rho_w} + g x_3 = 0 \qquad \text{in the fluid domain} \tag{2.16}$$

$\mathbf{x}$ is a spatial point, $\Phi = \Phi' + \int C(t)dt$ where Φ' is a potential, and $C(t)$ is a function of time. From the time harmonic assumption, the time related function can be excluded like (2.13).

2.3.1 Boundary conditions

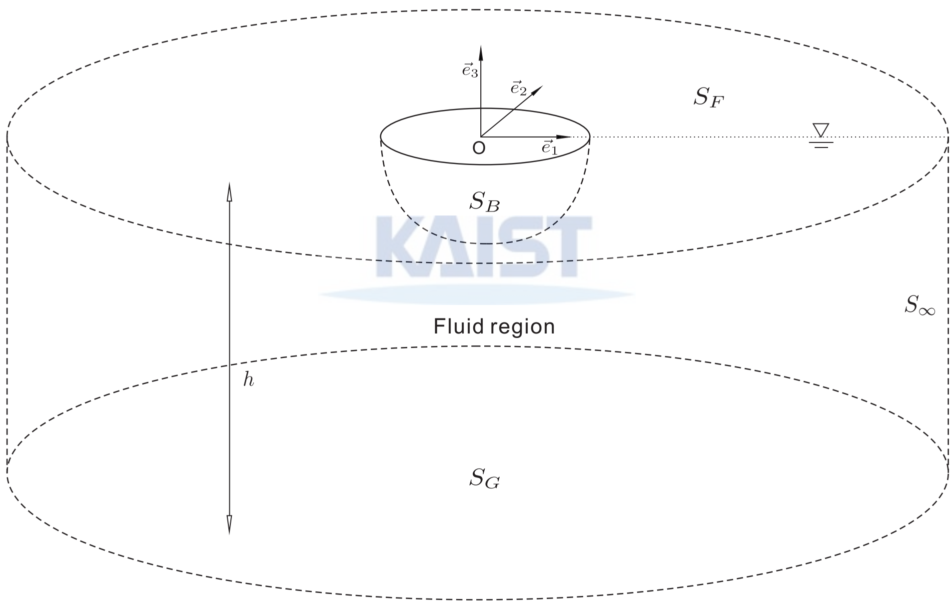

Figure 2.3: Schema of the fluid region

Fig. 2.3 represents the region of the fluid. S_B is the surface of interface between fluid and structure, S_F is the free surface, S_∞ is the surface that envelops the fluid region laterally, and S_G is the bottom surface.

On S_B, the normal velocity of the structure and the fluid should be same because if not the fluid would penetrate into the structure region and this situation is impossible. So we can give a condition (body boundary condition):

$$\frac{\partial \phi}{\partial n} = i\omega \mathbf{u} \cdot \mathbf{n} \qquad \text{on } S_B \tag{2.17}$$

where n is normal to S_B from the fluid region and $\mathbf{n}$ is corresponded unit vector.

On S_F, we can think two conditions. First if we observe the free surface with following it, it does not change. This is a similar explanation to the body boundary condition. Second the pressure is same with the given pressure distribution that we assume it is zero. Typically these two conditions are called "kinematic free surface boundary condition" and "dynamic free surface boundary condition". If we express these conditions mathematically, then

$$\frac{DF}{Dt} = 0 \qquad \text{on } S_F \tag{2.18}$$

$$\frac{\partial \Phi}{\partial t} + \frac{1}{2}\nabla\Phi \cdot \nabla\Phi + g x_3 = 0 \qquad \text{on } S_F \tag{2.19}$$

where $F \equiv x_3 - \zeta = 0$, ζ means the elevation of the free surface, and we neglect the surface tension effect. If we linearize (2.18) and (2.19) at $x_3 = 0$, then

$$\frac{\partial \phi}{\partial x_3} = i\omega\zeta \qquad \text{at } x_3 = 0 \text{ on } S_F \tag{2.20}$$

$$i\omega\phi = -g\zeta \qquad \text{at } x_3 = 0 \text{ on } S_F \tag{2.21}$$

If we combine the above equations, then we have

$$\frac{\partial \phi}{\partial x_3} = \frac{\omega^2}{g}\phi \qquad \text{at } x_3 = 0 \text{ on } S_F \tag{2.22}$$

You should be reminded that the linearized conditions, (2.20) and (2.21), are valid for waves with infinitesimally small amplitude and velocity.

On S_G, the same kinematic condition is applied. So if the bottom does not move, we obtain

$$\frac{\partial \phi}{\partial x_3} = 0 \qquad \text{on } S_G \tag{2.23}$$

Let's think the problem physically. The wave that is scattered from the structure and the wave caused by motion of the structure have a directivity. That is, they should be radiated from the structure's position to the infinity. This is called Sommerfeld radiation condition.

$$\lim_{R\to\infty} \sqrt{R}\left(\frac{\partial}{\partial R} + ik\right)(\phi - \phi_I) = 0 \tag{2.24}$$

where $R = \sqrt{(x_1^2 + x_2^2)}$, and k is the wave number. Because the Laplace's equation is linear, as you can see in (2.24), we can just represent the scattered and radiated potential as $\phi - \phi_I$ where $\Phi_I = \phi_I e^{i\omega t}$ and Φ_I is the velocity potential of the incident wave which satisfies all boundary condition except the body boundary condition and Sommerfeld radiation condition. The incident potential that the wave is coming from the positive $\mathbf{e}_1$ axis is

$$\Phi_I = i\frac{ga}{\omega}\frac{\cosh[k(x_3 + h)]}{\cosh(kh)} e^{ik[\cos(\theta x_1) + \sin(\theta x_2)]} e^{i\omega t} \tag{2.25}$$

for finite depth case

$$\Phi_I = i\frac{ga}{\omega} e^{kx_3} e^{ik[\cos(\theta x_1) + \sin(\theta x_2)]} e^{i\omega t} \tag{2.26}$$

for infinite depth case where a denotes the wave amplitude.

2.3.2 Green's function

The time harmonic free surface Green's function is a basis of this analysis. It is nothing but a kind of the source potential located at $\boldsymbol{\xi}$ that satisfies

$$
\begin{aligned}
\nabla^2 G &= 0 \qquad \text{for } -h \leqq x_3 \leqq 0 \text{ except at } \boldsymbol{\xi} \\
\frac{\partial G}{\partial x_3} &= \frac{\omega^2}{g} G \qquad \text{at } x_3 = 0 \\
\frac{\partial G}{\partial x_3} &= 0 \qquad \text{at } x_3 = -h \\
\lim_{R\to\infty} \sqrt{R}\left(\frac{\partial}{\partial R} + ik\right) G &= 0 \qquad \text{for } -h \leqq x_3 \leqq 0
\end{aligned} \tag{2.27}
$$

In infinite depth and finite depth with the source potential of strength -4π, it is defined by following expression [21]

$$
\begin{aligned}
G = & \frac{1}{\sqrt{R^2 + (x_3 - \xi_3)^2}} + P.V. \int_0^\infty \frac{k+K}{k-K} e^{-k|x_3+\xi_3|} J_0(kR) \mathrm{d}k \\
& - 2\pi K e^{-K|x_3+\xi_3|} J_0(KR) i
\end{aligned} \tag{2.28}
$$

for infinite depth case where $K = \frac{\omega^2}{g}$, J_0 is Bessel functions of the first kind of order 0, and $P.V.$ means the Cauchy principal value.

$$
\begin{aligned}
G = & \frac{1}{\sqrt{R^2 + (x_3 - \xi_3)^2}} + \frac{1}{\sqrt{R^2 + (2h + x_3 + \xi_3)^2}} \\
& + 2P.V. \int_0^\infty \frac{(k+K)\cosh k(x_3+h)\cosh k(\xi_3+h)}{k \sinh kh - K \cosh kh} e^{-kh} J_0(kR) \mathrm{d}k \\
& + 2\pi \frac{K^2 - k_0^2}{k_0^2 h - K^2 h + K} \cosh k_0(x_3+h) \cosh k_0(\xi_3+h) J_0(k_0 R) i
\end{aligned} \tag{2.29}
$$

for finite depth case where k_0 is the positive real root of the equation, $K = k\tanh(kh)$.

The derivatives of the Green's function are

$$
\begin{aligned}
\frac{\partial G}{\partial R} = & -\frac{R}{(R^2 + (x_3 - \xi_3)^2)^{\frac{3}{2}}} - K^2 \Big(\frac{R}{K^2 (R^2 + (x_3 + \xi_3)^2)^{\frac{3}{2}}} - \pi e^{-K|x_3+\xi_3|} (H_1(KR) + Y_1(KR) - \frac{2}{\pi}) \\
& + \frac{2e^{-K|x_3+\xi_3|}}{KR} \int_0^{K|x_3+\xi_3|} \frac{te^t}{\sqrt{(KR)^2 + t^2}} \mathrm{d}t - \frac{2|x_3+\xi_3|}{KR\sqrt{(R^2 + (x_3+\xi_3)^2}} \Big) \\
& + 2\pi K^2 e^{-K|x_3+\xi_3|} J_1(KR) i
\end{aligned} \tag{2.30}
$$

$$
\begin{aligned}
\frac{\partial G}{\partial \xi_3} = & -\frac{(\xi_3 - x_3)}{(R^2 + (x_3 - \xi_3)^2)^{\frac{3}{2}}} + K^2 \Big(\frac{1}{K\sqrt{R^2 + (x_3+\xi_3)^2}} \\
& + P.V. \int_0^\infty \frac{k+1}{k-1} e^{-kK|x_3+\xi_3|} J_0(kKR) \mathrm{d}k + \frac{|x_3+\xi_3|}{K^2 (R^2 + (x_3+\xi_3)^2)^{\frac{3}{2}}} \Big) \\
& - 2\pi K^2 e^{-K|x_3+\xi_3|} J_0(KR) i
\end{aligned} \tag{2.31}
$$

for infinite depth case where J_1, Y_1, and H_1 are Bessel functions of the first, second and Struve function of order 1 respectively, and

$$\frac{\partial G}{\partial R} = -\frac{R}{(R^2+(x_3-\xi_3)^2)^{\frac{3}{2}}} - \frac{R}{(R^2+(2h+x_3+\xi_3)^2)^{\frac{3}{2}}}$$
$$-2P.V.\int_0^\infty \frac{(k+K)\cosh k(x_3+h)\cosh k(\xi_3+h)}{k\sinh kh - K\cosh kh} e^{-kh} kJ_1(kR)\mathrm{d}k$$
$$-2\pi\frac{K^2-k_0^2}{k_0^2 h - K^2 h + K}\cosh k_0(x_3+h)\cosh k_0(\xi_3+h) k_0 J_1(k_0 R) i \tag{2.32}$$
$$\frac{\partial G}{\partial \xi_3} = -\frac{(\xi_3-x_3)}{(R^2+(x_3-\xi_3)^2)^{\frac{3}{2}}} - \frac{2h+x_3+\xi_3}{(R^2+(2h+x_3+\xi_3)^2)^{\frac{3}{2}}}$$
$$+2P.V.\int_0^\infty \frac{(k+K)\cosh k(x_3+h) k\sinh k(\xi_3+h)}{k\sinh kh - K\cosh kh} e^{-kh} J_0(kR)\mathrm{d}k$$
$$+2\pi\frac{K^2-k_0^2}{k_0^2 h - K^2 h + K}\cosh k_0(x_3+h) k_0 \sinh k_0(\xi_3+h) J_0(k_0 R) i \tag{2.33}$$

for finite depth case.

A special attention should be given to the Green's function. As you can see in this subsection, evaluating the Green's function doesn't come easy. To overcome the complexity of the Green's function, many researchers have found the other forms of it, but they are very slow to compute numerically. With based on these forms of the Green's function, a efficient algorithm [13] has developed to solve this extremely time-consuming problem , and we adopt this algorithm to compute the Green's function.

2.3.3 Boundary integral equation

Starting point is the Green's theorem. If two potentials denoted φ and ψ satisfy the Laplace's equation in the fluid region, it is easy to show that

$$\int_{S_C}\left(\varphi\frac{\partial\psi}{\partial n} - \psi\frac{\partial\varphi}{\partial n}\right) dS_C = 0 \tag{2.34}$$

where n is normal to S_C from the fluid region, and S_C is a smooth closed surface surrounding the fluid domain. When one of two potentials has points or regions where it does not satisfy the Laplace's equation, especially exhibits singularity, we can apply some technique to (2.34), and derive useful equations [9]. That equations are following:

$$\int_{S_C}\left(\phi(\boldsymbol{\xi})\frac{\partial G(\mathbf{x};\boldsymbol{\xi})}{\partial n(\boldsymbol{\xi})} - G(\mathbf{x};\boldsymbol{\xi})\frac{\partial \phi(\boldsymbol{\xi})}{\partial n(\boldsymbol{\xi})}\right)\mathrm{d}S_C(\boldsymbol{\xi}) = \begin{cases} 0 & \text{for } \mathbf{x} \text{ outside } S_C \\ -2\pi\phi(\mathbf{x}) & \text{for } \mathbf{x} \text{ on } S_C \\ -4\pi\phi(\mathbf{x}) & \text{for } \mathbf{x} \text{ inside } S_C \end{cases} \tag{2.35}$$

The right side of (2.35) comes from the contribution of the integration over very small surface that surrounds the point source singularity of the Green's function.

Consider first a volume V_O surrounded by S_B, S_{FO}, S_G, and S_∞ as shown in Fig.2.4. We can apply (2.35) to this region, and then obtain

$$-2\pi\phi(\mathbf{x}) = \int_{S_B+S_{FO}+S_G+S_\infty}\left(\phi(\boldsymbol{\xi})\frac{\partial G(\mathbf{x};\boldsymbol{\xi})}{\partial n(\boldsymbol{\xi})} - G(\mathbf{x};\boldsymbol{\xi})\frac{\partial \phi(\boldsymbol{\xi})}{\partial n(\boldsymbol{\xi})}\right)\mathrm{d}S_C(\boldsymbol{\xi}) \qquad \text{for } \mathbf{x} \text{ on } S_B \tag{2.36}$$

Because G has same boundary conditions with ϕ on S_{FO} and S_G,and with $\phi-\phi_I$ on S_∞, so we have

$$-2\pi\phi(\mathbf{x}) = \int_{S_B}\left(\phi(\boldsymbol{\xi})\frac{\partial G(\mathbf{x};\boldsymbol{\xi})}{\partial n(\boldsymbol{\xi})} - G(\mathbf{x};\boldsymbol{\xi})\frac{\partial \phi(\boldsymbol{\xi})}{\partial n(\boldsymbol{\xi})}\right)\mathrm{d}S_B(\boldsymbol{\xi})$$
$$+\int_{S_\infty}\left(\phi_I(\boldsymbol{\xi})\frac{\partial G(\mathbf{x};\boldsymbol{\xi})}{\partial n(\boldsymbol{\xi})} - G(\mathbf{x};\boldsymbol{\xi})\frac{\partial \phi_I(\boldsymbol{\xi})}{\partial n(\boldsymbol{\xi})}\right)\mathrm{d}S_\infty(\boldsymbol{\xi}) \qquad \text{for } \mathbf{x} \text{ on } S_B \tag{2.37}$$

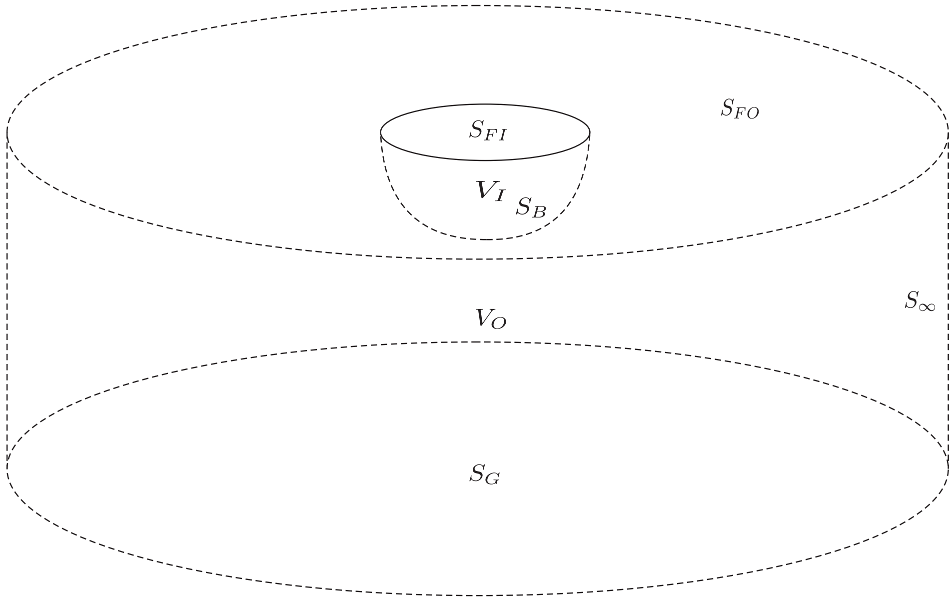

Figure 2.4: The fluid boundary description

If we apply same procedure to ϕ_I, then

$$\begin{aligned}-2\pi\phi_I(\mathbf{x}) = &\int_{S_B}\left(\phi_I(\boldsymbol{\xi})\frac{\partial G(\mathbf{x};\boldsymbol{\xi})}{\partial n(\boldsymbol{\xi})} - G(\mathbf{x};\boldsymbol{\xi})\frac{\partial \phi_I(\boldsymbol{\xi})}{\partial n(\boldsymbol{\xi})}\right)\mathrm{d}S_B(\boldsymbol{\xi})\\ &+\int_{S_\infty}\left(\phi_I(\boldsymbol{\xi})\frac{\partial G(\mathbf{x};\boldsymbol{\xi})}{\partial n(\boldsymbol{\xi})} - G(\mathbf{x};\boldsymbol{\xi})\frac{\partial \phi_I(\boldsymbol{\xi})}{\partial n(\boldsymbol{\xi})}\right)\mathrm{d}S_\infty(\boldsymbol{\xi}) \qquad \text{for } \mathbf{x} \text{ on } S_B \qquad (2.38)\end{aligned}$$

Next, subtract (2.38) from (2.37), then we get

$$\begin{aligned}-2\pi\phi(\mathbf{x}) + 2\pi\phi_I(\mathbf{x}) = &\int_{S_B}\left(\phi(\boldsymbol{\xi})\frac{\partial G(\mathbf{x};\boldsymbol{\xi})}{\partial n(\boldsymbol{\xi})} - G(\mathbf{x};\boldsymbol{\xi})\frac{\partial \phi(\boldsymbol{\xi})}{\partial n(\boldsymbol{\xi})}\right)\mathrm{d}S_B(\boldsymbol{\xi})\\ &-\int_{S_B}\left(\phi_I(\boldsymbol{\xi})\frac{\partial G(\mathbf{x};\boldsymbol{\xi})}{\partial n(\boldsymbol{\xi})} - G(\mathbf{x};\boldsymbol{\xi})\frac{\partial \phi_I(\boldsymbol{\xi})}{\partial n(\boldsymbol{\xi})}\right)\mathrm{d}S_B(\boldsymbol{\xi}) \qquad \text{for } \mathbf{x} \text{ on } S_B \qquad (2.39)\end{aligned}$$

We also think same process for ϕ_I in V_I because ϕ_I and G satisfy the Laplace's equation in V_I. So we can derive the following:

$$2\pi\phi_I(\mathbf{x}) = \int_{S_B}\left(\phi_I(\boldsymbol{\xi})\frac{\partial G(\mathbf{x};\boldsymbol{\xi})}{\partial n(\boldsymbol{\xi})} - G(\mathbf{x};\boldsymbol{\xi})\frac{\partial \phi_I(\boldsymbol{\xi})}{\partial n(\boldsymbol{\xi})}\right)\mathrm{d}S_B \qquad \text{for } \mathbf{x} \text{ on } S_B \qquad (2.40)$$

where the sign for $2\pi\phi_I(\mathbf{x})$ is plus because the normal direction 'n' is to S_B from V_O. So we finally obtain, if add (2.39) and (2.40)

$$-2\pi\phi(\mathbf{x}) + 4\pi\phi_I(\mathbf{x}) = \int_{S_B}\left(\phi(\boldsymbol{\xi})\frac{\partial G(\mathbf{x};\boldsymbol{\xi})}{\partial n(\boldsymbol{\xi})} - G(\mathbf{x};\boldsymbol{\xi})\frac{\partial \phi(\boldsymbol{\xi})}{\partial n(\boldsymbol{\xi})}\right)\mathrm{d}S_B(\boldsymbol{\xi}) \qquad \text{for } \mathbf{x} \text{ on } S_B \qquad (2.41)$$

and variational formulation:

$$\begin{aligned}&-\int_{S_B} 2\pi\phi(\mathbf{x})\bar{\phi}(\mathbf{x})dS_B(\mathbf{x}) + \int_{S_B} 4\pi\phi_I(\mathbf{x})\bar{\phi}(\mathbf{x})dS_B(\mathbf{x}) =\\ &\int_{S_B}\int_{S_B}\left(\phi(\boldsymbol{\xi})\frac{\partial G(\mathbf{x};\boldsymbol{\xi})}{\partial n(\boldsymbol{\xi})} - G(\mathbf{x};\boldsymbol{\xi})\frac{\partial \phi(\boldsymbol{\xi})}{\partial n(\boldsymbol{\xi})}\right)\mathrm{d}S_B(\boldsymbol{\xi})\bar{\phi}(\mathbf{x})\mathrm{d}S_B(\mathbf{x}) \qquad (2.42)\end{aligned}$$

where $\bar{\phi}$ means the virtual velocity potential.

(2.41) is similar with the classical approach [19]. In the classical point of view, ϕ is divided like

$$\phi = \phi_D + \phi_R \tag{2.43}$$

where

$$\phi_D = \phi_I + \phi_S \tag{2.44}$$

In above equations, ϕ_R means the potential caused by the motion of the structure and ϕ_S is the scattered potential by the incident wave when the structure is fixed. The body boundary condition becomes

$$\begin{aligned} \frac{\partial \phi_R}{\partial n} &= i\omega \mathbf{u} \cdot \mathbf{n} \qquad \text{on } S_B \\ \frac{\partial \phi_D}{\partial n} &= 0 \qquad \text{on } S_B \end{aligned} \tag{2.45}$$

If we try the same procedure as described previously, we have

$$-2\pi\phi_R(\mathbf{x}) = \int_{S_B} \left(\phi_R(\boldsymbol{\xi}) \frac{\partial G(\mathbf{x};\boldsymbol{\xi})}{\partial n(\boldsymbol{\xi})} - G(\mathbf{x};\boldsymbol{\xi}) \frac{\partial \phi_R(\boldsymbol{\xi})}{\partial n(\boldsymbol{\xi})} \right) \mathrm{d}S_B(\boldsymbol{\xi}) \qquad \text{for } \mathbf{x} \text{ on } S_B \tag{2.46}$$

and

$$-2\pi\phi_D(\mathbf{x}) + 4\pi\phi_I(\mathbf{x}) = \int_{S_B} \phi_D(\boldsymbol{\xi}) \frac{\partial G(\mathbf{x};\boldsymbol{\xi})}{\partial n(\boldsymbol{\xi})} \mathrm{d}S_B(\boldsymbol{\xi}) \qquad \text{for } \mathbf{x} \text{ on } S_B \tag{2.47}$$

Typically (2.46) and (2.47) are called "radiation problem" and "diffraction problem" respectively. The result of adding (2.46) and (2.47) is same with (2.41).

2.4 Coupled equations for the frequency analysis

Let's start with the variational formulations for the floating structure (2.14) and the fluid (2.42). Because of the body boundary condition (2.17), we can rewrite that equations as

$$-\int_{{}^tV} \omega^2 \rho_s \bar{\mathbf{u}}^T \mathbf{u} \, \mathrm{d}^tV + \int_{{}^tV} \bar{\boldsymbol{\epsilon}}^T \boldsymbol{\sigma} \, \mathrm{d}^tV = -\int_{{}^tS_B} i\omega\rho_w \phi \bar{\mathbf{u}}^T \mathbf{n} \, \mathrm{d}^tS_B - \int_{{}^tS_B} \rho_w g u_3 \bar{\mathbf{u}}^T \mathbf{n} \, \mathrm{d}^tS_B \tag{2.48}$$

and

$$-\int_{{}^tS_B} 2\pi\phi(\mathbf{x})\bar{\phi}(\mathbf{x})\mathrm{d}^tS_B(\mathbf{x}) + \int_{{}^tS_B} 4\pi\phi_I(\mathbf{x})\bar{\phi}(\mathbf{x})\mathrm{d}^tS_B(\mathbf{x}) = \int_{{}^tS_B}\int_{{}^tS_B} \left(\phi(\boldsymbol{\xi})\frac{\partial G(\mathbf{x};\boldsymbol{\xi})}{\partial n(\boldsymbol{\xi})} - i\omega G(\mathbf{x};\boldsymbol{\xi})\mathbf{u}(\boldsymbol{\xi})\cdot\mathbf{n}(\boldsymbol{\xi})\right)\mathrm{d}^tS_B(\boldsymbol{\xi})\bar{\phi}(\mathbf{x})\mathrm{d}^tS_B(\mathbf{x}) \tag{2.49}$$

Because the direction of the normal vector $\mathbf{n}$ in (2.48) and (2.49) is outward from the fluid domain, we put a minus sign into the right hand side of (2.48).

The actual volume and surface the structure occupies at time t changes periodically from the static equilibrium state, but because of the assumptions of small displacements the variation of that is very small. So we can assume that ${}^tV \approx V$ and ${}^tS_B \approx S_B$ where V and S_B are the volume and the surface in the static equilibrium state. Then the final form of coupled equations are

$$-\int_{V} \omega^2 \rho_s \bar{\mathbf{u}}^T \mathbf{u} \, \mathrm{d}V + \int_{V} \bar{\boldsymbol{\epsilon}}^T \boldsymbol{\sigma} \, \mathrm{d}V = -\int_{S_B} i\omega\rho_w \phi \bar{\mathbf{u}}^T \mathbf{n} \, \mathrm{d}S_B - \int_{S_B} \rho_w g u_3 \bar{\mathbf{u}}^T \mathbf{n} \, dS_B \tag{2.50}$$

and

$$-\int_{S_B} 2\pi\phi(\mathbf{x})\bar{\phi}(\mathbf{x})\mathrm{d}S_B(\mathbf{x}) + \int_{S_B} 4\pi\phi_I(\mathbf{x})\bar{\phi}(\mathbf{x})\mathrm{d}S_B(\mathbf{x}) = \int_{S_B}\int_{S_B} \left(\phi(\boldsymbol{\xi})\frac{\partial G(\mathbf{x};\boldsymbol{\xi})}{\partial n(\boldsymbol{\xi})} - i\omega G(\mathbf{x};\boldsymbol{\xi})\mathbf{u}(\boldsymbol{\xi})\cdot\mathbf{n}(\boldsymbol{\xi})\right)\mathrm{d}S_B(\boldsymbol{\xi})\bar{\phi}(\mathbf{x})\mathrm{d}S_B(\mathbf{x}) \tag{2.51}$$

Chapter 3. Numerical methods

In this chapter we apply (2.50) and (2.51) into shell structures. The basic assumption of the shell structures is that the undeformed material line initially normal to the midsurface of the shell structures keeps its straight and remains unstretched during the deformations [5]. With this shell structure, we discrete the domain of problem, i.e., finite shell elements for the structure and boundary elements for the fluid.

3.1 Shell elements for the structure

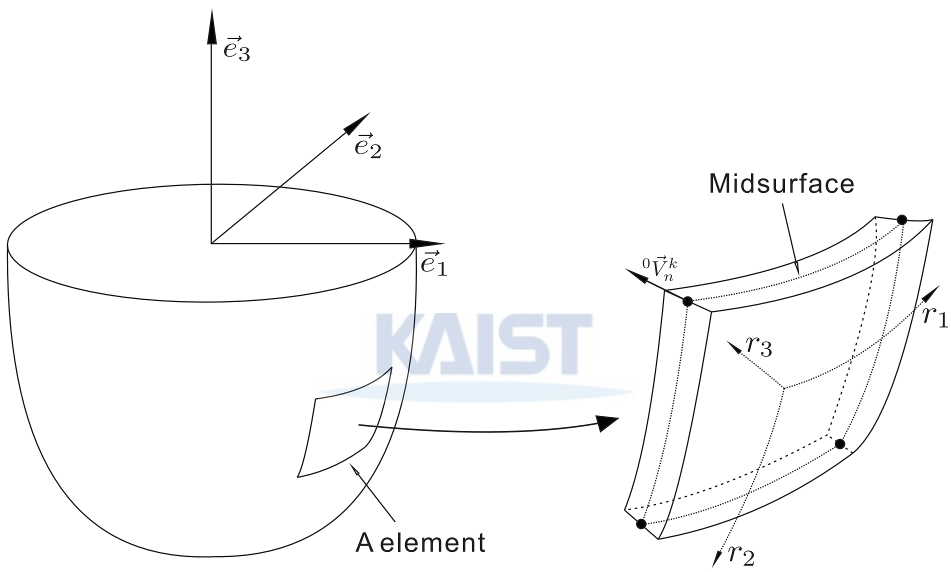

Figure 3.1: A shell element geometry

Let's consider the geometry of shell elements. Fig. 3.1 shows a four nodes shell element. With the assumption of the shell structures, which is mentioned before, we can represent a material point in the state equilibrium configuration ${}^0\mathbf{x}$ and a displacement $\mathbf{u}$ using the natural coordinate system r_1, r_2, and r_3 for a four node shell element

$$ {}^0\mathbf{x}(r_1, r_2, r_3) = \sum_{k=1}^{4} h_k(r_1, r_2)\,{}^0\mathbf{x}_k + \sum_{k=1}^{4} h_k(r_1, r_2)\frac{r_3 a_k}{2}\,{}^0\mathbf{V}_n^k \tag{3.1} $$

and

$$ \mathbf{u}(r_1, r_2, r_3) = \sum_{k=1}^{4} h_k(r_1, r_2)\mathbf{u}_k + \sum_{k=1}^{4} h_k(r_1, r_2)\frac{r_3 a_k}{2}\,\delta\mathbf{V}_n^k \tag{3.2} $$

where ${}^0\mathbf{x}_k$, a_k, ${}^0\mathbf{V}_n^k$, $\delta\mathbf{V}_n^k$, and h_k are the nodal material points vector, the nodal thickness of shell in r_3 direction, the nodal unit normal vector to the midsurface, the differences of ${}^t\mathbf{V}_n^k$ and ${}^0\mathbf{V}_n^k$, and the interpolation functions respectively.

From the assumption of small displacements, we can express $\delta\mathbf{V}_n^k$ like

$$ \delta\mathbf{V}_n^k = \beta_k\,{}^0\mathbf{V}_1^k - \alpha_k\,{}^0\mathbf{V}_2^k \tag{3.3} $$

where α_k and β_k are the rotations of ${}^0\mathbf{V}_n^k$ in the direction of ${}^0\mathbf{V}_1^k$ and ${}^0\mathbf{V}_2^k$ respectively. ${}^0\mathbf{V}_1^k$ and ${}^0\mathbf{V}_2^k$ are defined by

$$\begin{aligned} {}^0\mathbf{V}_1^k &\equiv \frac{\mathbf{e}_2 \times {}^0\mathbf{V}_n^k}{\| \mathbf{e}_2 \times {}^0\mathbf{V}_n^k \|_2} \\ {}^0\mathbf{V}_2^k &\equiv {}^0\mathbf{V}_n^k \times {}^0\mathbf{V}_1^k \end{aligned} \tag{3.4}$$

If ${}^0\mathbf{V}_n^k$ is parallel to $\mathbf{e}_2$, then we just set ${}^0\mathbf{V}_1^k$ equal to $\mathbf{e}_3$. So (3.2) becomes

$$\mathbf{u}(r_1, r_2, r_3) = \sum_{k=1}^{4} h_k(r_1, r_2)\mathbf{u}_k + \sum_{k=1}^{4} h_k(r_1, r_2)\frac{r_3 a_k}{2}(\beta_k\, {}^0\mathbf{V}_1^k - \alpha_k\, {}^0\mathbf{V}_2^k) \tag{3.5}$$

Before we apply finite element methods to the coupled equations using (3.1) and (3.5), there are important things that we shouldn't overlook. The first is that we have to consider the basic assumption of shell structure; i.e., the stress in the direction of thickness is zero, and the second is that we should avoid the shear locking phenomena. For the first thing we should transform the strain and the stress that are expressed in the global Cartesian coordinate system to the local Cartesian coordinate system. For the second thing we use the MITC4 elements proposed by Bathe K. J. and Dvorkin E. N. [2].

It is useful to introduce the covariant basis for applying above two procedures. The covariant base vectors are

$$\mathbf{g}_i = \frac{\partial^0\mathbf{x}}{\partial r_i} \tag{3.6}$$

and the corresponding contravariant vectors are $\mathbf{g}^i$ which have the relationships

$$\mathbf{g}_i \cdot \mathbf{g}^j = \delta_{ij} \tag{3.7}$$

where δ_{ij} is the Kronecker delta. So the strain tensor is expressed by

$$\boldsymbol{\epsilon} = \tilde{\epsilon}_{11}\mathbf{g}^1\mathbf{g}^1 + \tilde{\epsilon}_{22}\mathbf{g}^2\mathbf{g}^2 + \tilde{\epsilon}_{12}(\mathbf{g}^1\mathbf{g}^2 + \mathbf{g}^2\mathbf{g}^1) + \tilde{\epsilon}_{23}(\mathbf{g}^2\mathbf{g}^3 + \mathbf{g}^3\mathbf{g}^2) + \tilde{\epsilon}_{31}(\mathbf{g}^3\mathbf{g}^1 + \mathbf{g}^1\mathbf{g}^3) \tag{3.8}$$

where $\tilde{\epsilon}_{ij}$ mean the linear components of the covariant Green-Lagrange strain tensor, i.e.,

$$\tilde{\epsilon}_{ij} = \frac{1}{2}\left(\frac{\partial \mathbf{u}}{\partial r_i} \cdot \frac{\partial^0\mathbf{x}}{\partial r_j} + \frac{\partial^0\mathbf{x}}{\partial r_i} \cdot \frac{\partial \mathbf{u}}{\partial r_j}\right) \tag{3.9}$$

The key point of the MITC4 elements is that we interpolate the transverse shear strains differently than the other strains (the bending and the membrane strains) that are evaluated from the displacement interpolations. It means that we reconstruct the transverse shear stains as the evaluated transverse shear strains at particular points. That is

$$\begin{aligned} \tilde{\epsilon}_{23}(r_1, r_3) &= \frac{1}{2}(1 + r_1)\tilde{\epsilon}_{23}(1, 0, r_3) + \frac{1}{2}(1 - r_1)\tilde{\epsilon}_{23}(-1, 0, r_3) \\ \tilde{\epsilon}_{31}(r_2, r_3) &= \frac{1}{2}(1 + r_2)\tilde{\epsilon}_{31}(0, 1, r_3) + \frac{1}{2}(1 - r_2)\tilde{\epsilon}_{31}(0, -1, r_3) \end{aligned} \tag{3.10}$$

With the above strains, the constitutive tensor should contain the shell assumption. So in the relation $\boldsymbol{\sigma} = \mathbb{Q}^T\mathbb{C}\mathbb{Q}\boldsymbol{\epsilon}$, we use

$$\mathbb{C} = \frac{E}{1-\nu^2}\begin{bmatrix} 1 & \nu & 0 & 0 & 0 & 0 \\ \nu & 1 & 0 & 0 & 0 & 0 \\ 0 & 0 & 0 & 0 & 0 & 0 \\ 0 & 0 & 0 & \frac{1-\nu}{2} & 0 & 0 \\ 0 & 0 & 0 & 0 & \kappa\frac{1-\nu}{2} & 0 \\ 0 & 0 & 0 & 0 & 0 & \kappa\frac{1-\nu}{2} \end{bmatrix} \tag{3.11}$$

where E is Young's modulus, ν is Poisson's ratio, κ is shear correction factor, and $\boldsymbol{\sigma}$ and $\boldsymbol{\epsilon}$ are the stress vector and the engineering strain vector which are defined (2.8). Because the constitutive matrix $\mathbb{C}$ is defined in the local Cartesian coordinate system which contains the unit base vector tangent to r_3 line, we have to transform it to the global Cartesian coordinate system where the stress vectors and the strain vectors are defined, or the stress vectors and the strain vectors to the local Cartesian coordinate system. The matrix $\mathbb{Q}$ functions as a connection between these two coordinate system, i.e., it transform the local coordinate system to the global coordinate system.

The local Cartesian coordinate system can be defined by

$$\begin{aligned} \mathbf{e}_r &= \frac{\mathbf{g}_2 \times \mathbf{g}_3}{\| \mathbf{g}_2 \times \mathbf{g}_3 \|_2} \\ \mathbf{e}_s &= \frac{\mathbf{g}_3 \times \mathbf{e}_r}{\| \mathbf{g}_3 \times \mathbf{e}_r \|_2} \\ \mathbf{e}_t &= \frac{\mathbf{g}_3}{\| \mathbf{g}_3 \|_2} \end{aligned} \tag{3.12}$$

and the transformation matrix $\mathbb{Q}$ is

$$\mathbb{Q} = \begin{bmatrix} R_{11}^2 & R_{21}^2 & R_{31}^2 & R_{11}R_{21} & R_{21}R_{31} & R_{31}R_{11} \\ R_{12}^2 & R_{22}^2 & R_{32}^2 & R_{12}R_{22} & R_{22}R_{32} & R_{32}R_{12} \\ R_{13}^2 & R_{23}^2 & R_{33}^2 & R_{13}R_{21} & R_{23}R_{33} & R_{33}R_{13} \\ 2R_{11}R_{12} & 2R_{21}R_{22} & 2R_{31}R_{32} & R_{11}R_{22}+R_{12}R_{21} & R_{21}R_{32}+R_{22}R_{31} & R_{31}R_{12}+R_{32}R_{11} \\ 2R_{12}R_{13} & 2R_{22}R_{23} & 2R_{32}R_{33} & R_{12}R_{23}+R_{13}R_{22} & R_{22}R_{33}+R_{23}R_{32} & R_{32}R_{13}+R_{33}R_{12} \\ 2R_{13}R_{11} & 2R_{23}R_{21} & 2R_{33}R_{31} & R_{13}R_{21}+R_{11}R_{23} & R_{23}R_{31}+R_{21}R_{33} & R_{33}R_{11}+R_{31}R_{13} \end{bmatrix} \tag{3.13}$$

where

$$\mathbb{R} = \begin{bmatrix} \mathbf{e}_1 \cdot \mathbf{e}_r & \mathbf{e}_1 \cdot \mathbf{e}_s & \mathbf{e}_1 \cdot \mathbf{e}_t \\ \mathbf{e}_2 \cdot \mathbf{e}_r & \mathbf{e}_2 \cdot \mathbf{e}_s & \mathbf{e}_2 \cdot \mathbf{e}_t \\ \mathbf{e}_3 \cdot \mathbf{e}_r & \mathbf{e}_3 \cdot \mathbf{e}_s & \mathbf{e}_3 \cdot \mathbf{e}_t \end{bmatrix} \tag{3.14}$$

3.2 Boundary elements for the fluid

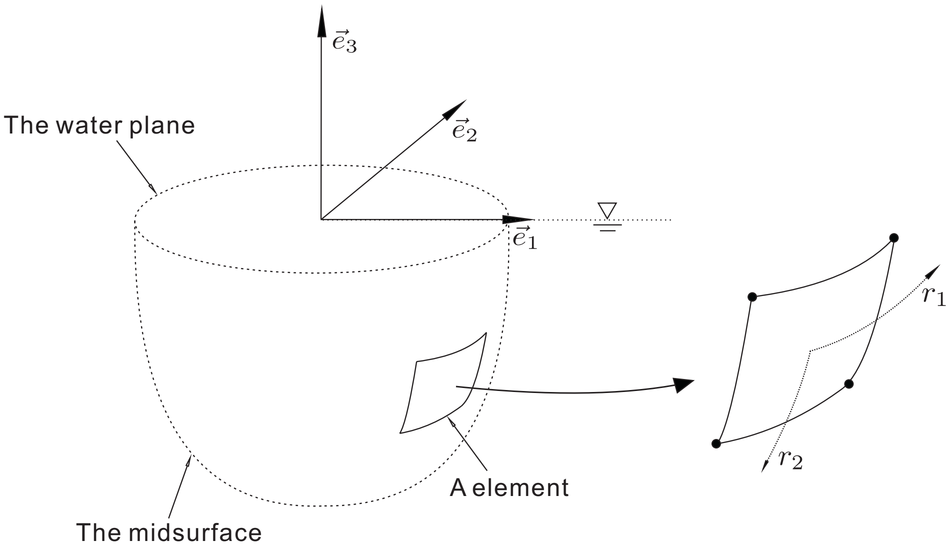

Figure 3.2: A boundary element geometry

Fig. 3.2 shows a four nodes boundary element of fluid. The boundary surface is the midsurface of the shell structure in the statically equilibrium state. Because the thickness of shell structure is small, there is no big difference when we take the midsurface as the boundary surface instead of actual wet surface. This is for efficient computation of the coupled equations.

Now we can interpolate the velocity potential on the body boundary for a four nodes boundary element like

$$\phi(r_1, r_2) = \sum_{k=1}^{4} h_k \phi^k \tag{3.15}$$

where ϕ^k is the nodal velocity potential. The unit normal vector can be obtained by

$$\mathbf{n}(r_1, r_2) = \frac{\mathbf{g}_1 \times \mathbf{g}_2}{\| \mathbf{g}_1 \times \mathbf{g}_2 \|_2} \tag{3.16}$$

The value of (3.16) is not exactly same with $\mathbf{e}_t$, but this does not cause big problems in our analysis. The reason why we define the normal vector differently than it in the shell structure is the evaluations of the integrations of the singularities that the Green's function has, which we will explain later.

3.3 Discrete version of the coupled equations

By dividing the structural domain and the fluid boundary domain into finite shell elements and boundary elements respectively, we can proceed to transform the coupled equations to a matrix form. So If we divide the structural volume into N elements and the body boundary surface into M elements, then (2.50) becomes

$$
\begin{aligned}
&-\int_V \omega^2 \rho_s \bar{\mathbf{u}}^T \mathbf{u}\, \mathrm{d}V + \int_V \bar{\boldsymbol{\epsilon}}^T \boldsymbol{\sigma}\, \mathrm{d}V + \int_{S_B} i\omega\rho_w \phi \bar{\mathbf{u}}^T \mathbf{n}\, \mathrm{d}S_B + \int_{S_B} \rho_w g u_3 \bar{\mathbf{u}}^T \mathbf{n}\, \mathrm{d}S_B = \\
&-\sum_{e=1}^{N}\left[\int_{V^e} \omega^2 \rho_s\, {}_e\bar{\mathbf{u}}^T\, {}_e\mathbf{u}\, \mathrm{d}V^e + \int_{V^e} {}_e\bar{\boldsymbol{\epsilon}}^T\, {}_e\boldsymbol{\sigma}\, \mathrm{d}V^e\right] + \sum_{e=1}^{M}\left[\int_{S_B^e} i\omega\rho_w\, {}_e\phi\, {}_e\bar{\mathbf{u}}^T \mathbf{n}\, \mathrm{d}S_B^e + \int_{S_B^e} \rho_w g\, {}_e u_3\, {}_e\bar{\mathbf{u}}^T \mathbf{n}\, \mathrm{d}S_B^e\right] = \\
&-\sum_{e=1}^{N}\left[{}_e\hat{\mathbf{u}}^T \int_{-1}^{1}\int_{-1}^{1}\int_{-1}^{1} \omega^2\rho_s \mathbb{H}^T\mathbb{H}\, \det(\mathbb{J})\mathrm{d}r_1\mathrm{d}r_2\mathrm{d}r_3\, {}_e\hat{\mathbf{u}} + {}_e\hat{\mathbf{u}}^T \int_{-1}^{1}\int_{-1}^{1}\int_{-1}^{1} \mathbb{B}^T\mathbb{Q}^T\mathbb{C}\mathbb{Q}\mathbb{B}\det(\mathbb{J})\mathrm{d}r_1\mathrm{d}r_2\mathrm{d}r_3\, {}_e\hat{\mathbf{u}}\right] \\
&+\sum_{e=1}^{M}\left[{}_e\hat{\mathbf{u}}^T \int_{-1}^{1}\int_{-1}^{1} i\omega\rho_w \mathbb{H}^T\mathbf{n}\mathbf{h}^T \parallel \mathbf{g}_1\times\mathbf{g}_2 \parallel_2 \mathrm{d}r_1\mathrm{d}r_2\, {}_e\hat{\boldsymbol{\phi}} + {}_e\hat{\mathbf{u}}^T \int_{-1}^{1}\int_{-1}^{1} \rho_w g \mathbb{H}^T\mathbf{n}\mathbf{h}_3^T \parallel \mathbf{g}_1\times\mathbf{g}_2 \parallel_2 \mathrm{d}r_1\mathrm{d}r_2\, {}_e\hat{\mathbf{u}}\right] = \\
&0
\end{aligned} \tag{3.17}
$$

and (2.51) is

$$
\begin{aligned}
&\int_{S_B} 2\pi\phi(\mathbf{x})\bar{\phi}(\mathbf{x})\,\mathrm{d}S_B(\mathbf{x}) - \int_{S_B} 4\pi\phi_I(\mathbf{x})\bar{\phi}(\mathbf{x})\,\mathrm{d}S_B(\mathbf{x}) \\
&+\int_{S_B}\int_{S_B}\left(\phi(\boldsymbol{\xi})\frac{\partial G(\mathbf{x};\boldsymbol{\xi})}{\partial n(\boldsymbol{\xi})} - i\omega G(\mathbf{x};\boldsymbol{\xi})\mathbf{u}(\boldsymbol{\xi})\cdot\mathbf{n}(\boldsymbol{\xi})\right)\mathrm{d}S_B(\boldsymbol{\xi})\,\bar{\phi}(\mathbf{x})\,\mathrm{d}^t S_B(\mathbf{x}) = \\
&\sum_{e=1}^{M}\left[{}_e\hat{\bar{\boldsymbol{\phi}}}^T \int_{-1}^{1}\int_{-1}^{1} 2\pi\mathbf{h}\mathbf{h}^T \parallel \mathbf{g}_1\times\mathbf{g}_2 \parallel_2 \mathrm{d}r_1\mathrm{d}r_2\, {}_e\hat{\boldsymbol{\phi}} - {}_e\hat{\bar{\boldsymbol{\phi}}}^T \int_{-1}^{1}\int_{-1}^{1} \phi_I \parallel \mathbf{g}_1\times\mathbf{g}_2 \parallel_2 \mathrm{d}r_1\mathrm{d}r_2\right] \\
&+\sum_{e=1}^{M}\sum_{\acute{e}=1}^{M}\left[{}_e\hat{\bar{\boldsymbol{\phi}}}^T \int_{-1}^{1}\int_{-1}^{1} \mathbf{h}\left(\int_{-1}^{1}\int_{-1}^{1} \mathbf{n}\cdot\nabla_{\boldsymbol{\xi}} G(r_1,r_2;\acute{r}_1,\acute{r}_2)\mathbf{h}^T \parallel \mathbf{g}_1\times\mathbf{g}_2 \parallel_2 \mathrm{d}\acute{r}_1\mathrm{d}\acute{r}_2\right) \parallel \mathbf{g}_1\times\mathbf{g}_2 \parallel_2 \mathrm{d}r_1\mathrm{d}r_2\, {}_{\acute{e}}\hat{\boldsymbol{\phi}}\right] \\
&-\sum_{e=1}^{M}\sum_{\acute{e}=1}^{M}\left[{}_e\hat{\bar{\boldsymbol{\phi}}}^T \int_{-1}^{1}\int_{-1}^{1} \mathbf{h}\left(\int_{-1}^{1}\int_{-1}^{1} i\omega G(r_1,r_2;\acute{r}_1,\acute{r}_2)\mathbf{h}_n^T \parallel \mathbf{g}_1\times\mathbf{g}_2 \parallel \mathrm{d}\acute{r}_1\mathrm{d}\acute{r}_2\right) \parallel \mathbf{g}_1\times\mathbf{g}_2 \parallel_2 \mathrm{d}r_1\mathrm{d}r_2\, {}_{\acute{e}}\hat{\mathbf{u}}\right] = 0
\end{aligned} \tag{3.18}
$$

where

$$
\begin{aligned}
{}_e\hat{\mathbf{u}}^T &= [{}_e\mathbf{u}_1^T \quad {}_e\alpha_1 \quad {}_e\beta_1 \quad {}_e\mathbf{u}_2^T \quad {}_e\alpha_2 \quad {}_e\beta_2 \quad {}_e\mathbf{u}_3^T \quad {}_e\alpha_3 \quad {}_e\beta_3 \quad {}_e\mathbf{u}_4^T \quad {}_e\alpha_4 \quad {}_e\beta_4] \\
{}_e\hat{\boldsymbol{\phi}}^T &= [{}_e\phi^1 \quad {}_e\phi^2 \quad {}_e\phi^3 \quad {}_e\phi^4] \\
{}_e\mathbf{u}(r_1,r_2,r_3) &= \mathbb{H}\, {}_e\hat{\mathbf{u}} \\
{}_e\boldsymbol{\epsilon}(r_1,r_2,r_3) &= \mathbb{B}\, {}_e\hat{\mathbf{u}} \\
{}_e u_3(r_1,r_2) &= \mathbf{h}_3^T\, {}_e\hat{\mathbf{u}} \\
{}_e\phi(r_1,r_2) &= \mathbf{h}^T\, {}_e\hat{\boldsymbol{\phi}} \\
{}_e\mathbf{u}\cdot\mathbf{n}(r_1,r_2) &= \mathbf{h}_n^T\, {}_e\hat{\mathbf{u}} \\
\frac{\partial}{\partial\mathbf{r}} &= \mathbb{J}\frac{\partial}{\partial\,{}^0\mathbf{x}}; \qquad \mathbf{r}^T = [r_1 \quad r_2 \quad r_3]
\end{aligned} \tag{3.19}
$$

Then we can obtain

$$
\begin{bmatrix} -\mathbb{S}_M + \mathbb{S}_K + \mathbb{S}_F & \mathbb{S}_C \\ -\mathbb{F}_G & \mathbb{F}_M + \mathbb{F}_{Gn} \end{bmatrix} \begin{bmatrix} \hat{\mathbf{u}} \\ \hat{\boldsymbol{\phi}} \end{bmatrix} = \begin{bmatrix} 0 \\ \mathbf{F}_I \end{bmatrix} \tag{3.20}
$$

where

$$
\begin{aligned}
\hat{\mathbf{u}}^T &= [\mathbf{u}_1^T \quad \alpha_1 \quad \beta_1 \quad \mathbf{u}_2^T \quad \alpha_2 \quad \beta_2 \quad \cdots \quad \mathbf{u}_N^T \quad \alpha_N \quad \beta_N] \\
\hat{\boldsymbol{\phi}}^T &= [\phi^1 \quad \phi^2 \quad \cdots \quad \phi^M] \\
\hat{\mathbf{u}}^T \mathbb{S}_M \hat{\mathbf{u}} &= \sum_{e=1}^{N} \left[{}_e\hat{\mathbf{u}}^T \int_{-1}^{1}\int_{-1}^{1}\int_{-1}^{1} \omega^2 \rho_s \mathbb{H}^T \mathbb{H} \det(\mathbb{J}) \mathrm{d}r_1 \mathrm{d}r_2 \mathrm{d}r_3 \, {}_e\hat{\mathbf{u}} \right] \\
\hat{\mathbf{u}}^T \mathbb{S}_K \hat{\mathbf{u}} &= \sum_{e=1}^{N} \left[{}_e\hat{\mathbf{u}}^T \int_{-1}^{1}\int_{-1}^{1}\int_{-1}^{1} \mathbb{B}^T \mathbb{Q}^T \mathbb{C} \mathbb{Q} \mathbb{B} \det(\mathbb{J}) \mathrm{d}r_1 \mathrm{d}r_2 \mathrm{d}r_3 \, {}_e\hat{\mathbf{u}} \right] \\
\hat{\mathbf{u}}^T \mathbb{S}_F \hat{\mathbf{u}} &= \sum_{e=1}^{M} \left[{}_e\hat{\mathbf{u}}^T \int_{-1}^{1}\int_{-1}^{1} \rho_w g \mathbb{H}^T \mathbf{n}\mathbf{h}_3^T \parallel \mathbf{g}_1 \times \mathbf{g}_2 \parallel_2 \mathrm{d}r_1 \mathrm{d}r_2 \, {}_e\hat{\mathbf{u}} \right] \\
\hat{\mathbf{u}}^T \mathbb{S}_F \hat{\boldsymbol{\phi}} &= \sum_{e=1}^{M} \left[{}_e\hat{\mathbf{u}}^T \int_{-1}^{1}\int_{-1}^{1} i\omega \rho_w \mathbb{H}^T \mathbf{n}\mathbf{h}^T \parallel \mathbf{g}_1 \times \mathbf{g}_2 \parallel_2 \mathrm{d}r_1 \mathrm{d}r_2 \, {}_e\hat{\boldsymbol{\phi}} \right] \\
\hat{\boldsymbol{\phi}}^T \mathbb{F}_G \hat{\mathbf{u}} &= \sum_{e=1}^{M}\sum_{\acute{e}=1}^{M} \left[{}_e\hat{\boldsymbol{\phi}}^T \int_{-1}^{1}\int_{-1}^{1} \mathbf{h} \left(\int_{-1}^{1}\int_{-1}^{1} i\omega G(r_1, r_2; \acute{r}_1, \acute{r}_2) \mathbf{h}_n^T \parallel \mathbf{g}_1 \times \mathbf{g}_2 \parallel \mathrm{d}\acute{r}_1 \mathrm{d}\acute{r}_2 \right) \parallel \mathbf{g}_1 \times \mathbf{g}_2 \parallel_2 \mathrm{d}r_1 \mathrm{d}r_2 \, {}_{\acute{e}}\hat{\mathbf{u}} \right] \\
\hat{\boldsymbol{\phi}}^T \mathbb{F}_{Gn} \hat{\boldsymbol{\phi}} &= \sum_{e=1}^{M}\sum_{\acute{e}=1}^{M} \left[{}_e\hat{\boldsymbol{\phi}}^T \int_{-1}^{1}\int_{-1}^{1} \mathbf{h} \left(\int_{-1}^{1}\int_{-1}^{1} \mathbf{n} \cdot \nabla_{\boldsymbol{\xi}} G(r_1, r_2; \acute{r}_1, \acute{r}_2) \mathbf{h}^T \parallel \mathbf{g}_1 \times \mathbf{g}_2 \parallel_2 \mathrm{d}\acute{r}_1 \mathrm{d}\acute{r}_2 \right) \parallel \mathbf{g}_1 \times \mathbf{g}_2 \parallel_2 \mathrm{d}r_1 \mathrm{d}r_2 \, {}_{\acute{e}}\hat{\boldsymbol{\phi}} \right] \\
\hat{\boldsymbol{\phi}}^T \mathbb{F}_M \hat{\boldsymbol{\phi}} &= \sum_{e=1}^{M} \left[{}_e\hat{\boldsymbol{\phi}}^T \int_{-1}^{1}\int_{-1}^{1} 2\pi \mathbf{h}\mathbf{h}^T \parallel \mathbf{g}_1 \times \mathbf{g}_2 \parallel_2 \mathrm{d}r_1 \mathrm{d}r_2 \, {}_e\hat{\boldsymbol{\phi}} \right] \\
\hat{\boldsymbol{\phi}}^T \mathbf{F}_I &= \sum_{e=1}^{M} \left[{}_e\hat{\boldsymbol{\phi}}^T \int_{-1}^{1}\int_{-1}^{1} \phi_I \parallel \mathbf{g}_1 \times \mathrm{g}_2 \parallel_2 \mathrm{d}r_1 \mathrm{d}r_2 \right]
\end{aligned} \tag{3.21}
$$

In the final linear system (3.21), the coefficient matrix is non-Hermitian matrix, so we use the flexible Generalized RESidual method which is kind of the projection method using a Krylov subspace to solve this system with variable preconditioning [16] [17]. We use the right preconditioned GMRES as a preconditioner at each step of the Arnoldi process. We find that the convergence for the linear system (3.21) is mainly influenced by the right preconditioner of GMRES. The generally used preconditioner, Incomplete LU factorization with no fill-in and the dual threshold incomplete LU factorization, denoted ILU(0) and ILUT respectively, did not work well, so we just use the IKJ version of Gaussian elimination as the right preconditioner with some modifications. But this is inefficient for very large system, so it is another issue.

3.4 Dealing with the singularities

Because the Green's function exhibits the singularity when the distance of the spatial point $\mathbf{x}$ and the source point $\boldsymbol{\xi}$ is very short, we have to pay attention to the integrations of it and it's derivative. One of the methods to overcome this integrations is well explained in [19], and we adopt it. It is that the singular components are separated from the Green's function, then integrations of that are evaluated in a special manner and then because the rest is regular we can use the Gauss-Legendre quadrature.

The Green's function can be divided by [10]

$$G(\mathbf{x};\boldsymbol{\xi}) = S_1 + S_2 + S_3 + \tilde{G} \tag{3.22}$$

and

$$\nabla_\xi G(\mathbf{x};\boldsymbol{\xi}) = \mathbf{S}_1 + \mathbf{S}_2 + \mathbf{S}_3 + \nabla_\xi \tilde{G} \tag{3.23}$$

where

$$\begin{aligned}
r &= \sqrt{(x_1-\xi_1)^2+(x_2-\xi_2)^2+(x_3-\xi_3)^2} \\
r' &= \sqrt{(x_1-\xi_1)^2+(x_2-\xi_2)^2+(x_3+\xi_3)^2} \\
S_1 &= \frac{1}{r}; \quad \mathbf{S}_1 = \nabla_\xi S_1 \\
S_2 &= \frac{1}{r'}; \quad \mathbf{S}_2 = \nabla_\xi S_2 \\
S_3 &= 2Ke^{K(x_3+\xi_3)}\ln[r'-(x_3+\xi_3)]; \quad \mathbf{S}_3 = \nabla_\xi S_3 \\
\tilde{G} \quad &\text{and} \quad \nabla_\xi \tilde{G} \;:\; \text{the regular part of the Green's function}
\end{aligned} \tag{3.24}$$

The singular or nearly singular components of the Green's function, shown in (3.22) and (3.23) are depend on the distance between $\mathbf{x}$ and $\boldsymbol{\xi}$, so we set up the following algorithm which is almost same with [19]. This is for evaluating the integration of these components.

Table 3.1: A algorithm for integration of the singular components

when $e = é$	when $e \neq é$
If x_3 and $\xi_3 = 0$ S_1, S_2, S_3 : singular integral	If $\frac{l_é}{l_p} > 0.5$ and $\frac{l_é}{l_{p'}} > 0.5$ S_1, S_2, S_3 : subdivided domain integral
Else if $\frac{l_é}{l_{p'}} > 0.5$ S_1 : singular integral S_2, S_3 : subdivided domain integral	Else if $\frac{l_é}{l_p} > 0.5$ and $\frac{l_é}{l_{p'}} \leq 0.5$ S_1 : subdivided domain integral
Else S_1 : singular integral	Else if $\frac{l_é}{l_p} \leq 0.5$ and $\frac{l_é}{l_{p'}} > 0.5$ S_2, S_3 : subdivided domain integral

In Table 3.1, e denotes a element where $\mathbf{x}$ is defined, e' is where $\boldsymbol{\xi}$ belongs to, $l_é$ is half length of the element e' diagonal. The distance between the spatial position $\mathbf{x}$ and the centroid of the element e' is defined by l_p, and between the point $(x_1, x_2, -x_3)$ and the centroid of the element e' by $l_{p'}$.

The subdivided domain integral is nothing but the element e' is subdivided until the distance ratio is smaller than some particular value. The distance ratio is $l_é$ to l_p for S_1, and $l_é$ to $l_{p'}$ for S_2 and S_3. You should be reminded that $l_é$, l_p, and $l_{p'}$ correspond to the subdivided element. The critical value that stops subdividing depend on your design criteria, but we choose 0.5 for it because approximately this value gives reliable results when using four points Gauss-Legendre quadrature.

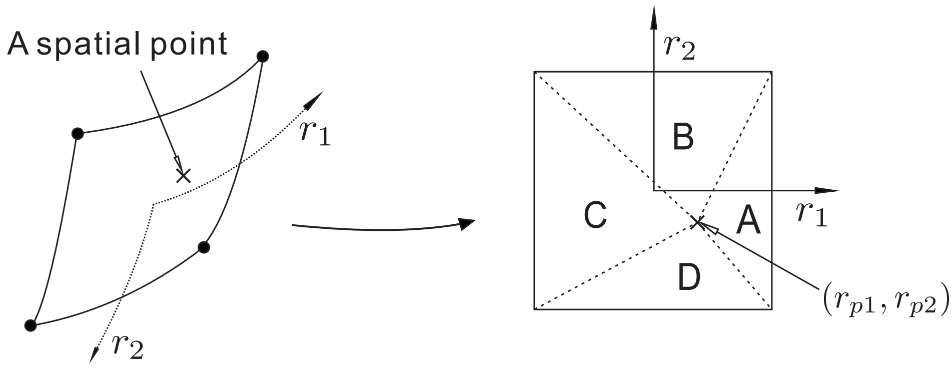

Figure 3.3: Separating a domain for the singular integrals

To understand the singular integral, consider Fig. 3.3 where a spatial point $\mathbf{x}^p$ is in the element that we are going to compute. The singular integrals we have to evaluate are classed as

$$\begin{aligned}
\int_{-1}^{1}\int_{-1}^{1} f\frac{1}{\parallel \mathbf{R} \parallel_2}\mathrm{d}r_1\mathrm{d}r_2 J \quad &: \quad \text{the source type} \\
\int_{-1}^{1}\int_{-1}^{1} f\frac{\mathbf{n}\cdot\mathbf{R}}{(\parallel \mathbf{R} \parallel_2)^3}\mathrm{d}r_1\mathrm{d}r_2 J \quad &: \quad \text{the dipole type} \\
\int_{-1}^{1}\int_{-1}^{1} f\ln(\parallel \mathbf{R} \parallel_2)\mathrm{d}r_1\mathrm{d}r_2 J \quad &: \quad \text{the logarithmic type}
\end{aligned} \tag{3.25}$$

where

$$\begin{aligned}
\mathbf{R} &= \mathbf{x} - \mathbf{x}^p \\
\mathbf{n} &= \frac{\frac{\partial \mathbf{x}}{\partial r_1} \times \frac{\partial \mathbf{x}}{\partial r_2}}{J} \\
J &= \parallel \frac{\partial \mathbf{x}}{\partial r_1} \times \frac{\partial \mathbf{x}}{\partial r_2} \parallel_2 \\
f \quad &: \quad \text{a regular function}
\end{aligned} \tag{3.26}$$

We have interpolated like

$$\begin{aligned}
\mathbf{x} &= \sum_{k=1}^{4} h_k \mathbf{x}^k \\
&= \mathbf{C}^{r_1 r_2} r_1 r_2 + \mathbf{C}^{r_1} r_1 + \mathbf{C}^{r_2} r_2 + \mathbf{C}
\end{aligned} \tag{3.27}$$

where, $\mathbf{C}^{r_1 r_2}$, $\mathbf{C}^{r_1}$, and $\mathbf{C}^{r_2}$ are corresponding coefficient vectors. So we get

$$\mathbf{R} = \mathbf{C}^{r_1 r_2}(r_1 r_2 - r_{p1} r_{p2}) + \mathbf{C}^{r_1}(r_1 - r_{p1}) + \mathbf{C}^{r_2}(r_2 - r_{p2}) \tag{3.28}$$

and

$$\mathbf{n}\cdot\mathbf{R} = \frac{\mathbf{C}^{r_1 r_2} \times \mathbf{C}^{r_2} \cdot \mathbf{C}^{r_1}(r_1 r_2 - r_{p1} r_2 - r_{p2} r_1 + r_{p1} r_{p2})}{J} \tag{3.29}$$

With (3.28) and (3.29), If we assume like

$$u \equiv r_1 - r_{p1};\ uv \equiv r_2 - r_{p2} \quad \text{in the region A} \tag{3.30}$$

then (3.25) becomes

$$\int_0^{1-r_{p1}} \int_{\frac{-1-r_{p2}}{1-r_{p1}}}^{\frac{1-r_{p2}}{1-r_{p1}}} f \frac{J}{\| \mathbf{C}^{r_1 r_2}(uv + vr_{p1} + r_{p2}) + \mathbf{C}^{r_1} + \mathbf{C}^{r_2} v \|_2} \mathrm{d}v\mathrm{d}u$$

$$\int_0^{1-r_{p1}} \int_{\frac{-1-r_{p2}}{1-r_{p1}}}^{\frac{1-r_{p2}}{1-r_{p1}}} -f \frac{\mathbf{C}^{r_1 r_2} \times \mathbf{C}^{r_2} \cdot \mathbf{C}^{r_1} v}{(\| \mathbf{C}^{r_1 r_2}(uv + vr_{p1} + r_{p2}) + \mathbf{C}^{r_1} + \mathbf{C}^{r_2} v \|_2)^3} \mathrm{d}v\mathrm{d}u$$

$$\int_0^{1-r_{p1}} \int_{\frac{-1-r_{p2}}{1-r_{p1}}}^{\frac{1-r_{p2}}{1-r_{p1}}} f J u \ln(\| \mathbf{C}^{r_1 r_2}(uv + vr_{p1} + r_{p2}) + \mathbf{C}^{r_1} + \mathbf{C}^{r_2} v \|_2 \, u) \mathrm{d}v\mathrm{d}u \quad \text{in the region A} \tag{3.31}$$

respectively. The worthy of notice in (3.31) is that the singular integrals become regular integrals, so we can apply the Gauss-Legendre quadrature for evaluations. The other regions also could be changed by same procedure, but the substitution variables are different according to the region, i.e.,

$$\begin{aligned} &u \equiv r_1 - r_{p1};\ uv \equiv r_2 - r_{p2} \quad \text{in the region A and C} \\ &uv \equiv r_1 - r_{p1};\ u \equiv r_2 - r_{p2} \quad \text{in the region B and D} \end{aligned} \tag{3.32}$$

Chapter 4. Results

In this chapter, we validate our mathematical formulation by comparing with an experiment result. We also compute additional two models, a box-like model and a Wigley hull, and include the behaviors of that.

4.1 Comparison with the experiment of a plate model

To validate the numerical formulation, it is recommended to compare with a experiment result. Fortunately there is a experiment result for hydroelastic response of a mat-like floating structure in regular waves. It is carried out by Yago K. and Endo H. [22] and the test description is in Fig. 4.1 and Table 4.1.

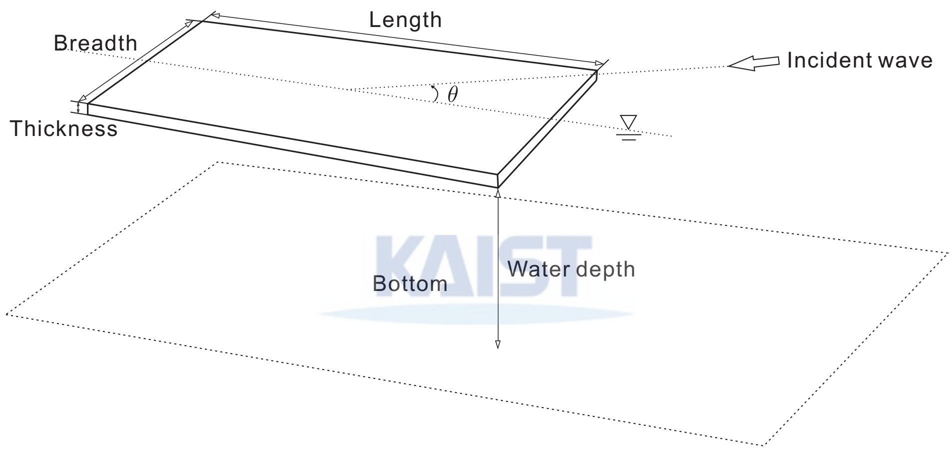

Figure 4.1: Schema of the experimental model [Yago K. and Endo H. (1996)]

Table 4.1: The test model description [Yago K. and Endo H. (1996)]

	Test model	Prototype
Scale ratio	$\frac{1}{30.77}$	1
Length (L)	9.75m	300m
Breadth (B)	1.9m	60m
Thickness (T)	0.0545m	2m
Stiffness (EI)	$1.788 \times 10^3 \mathrm{kgf} \cdot \mathrm{m}^2$	$4.87 \times 10^{10} \mathrm{kgf} \cdot \mathrm{m}^2$

Water Depth	1.9m
$\frac{\lambda}{\mathrm{L}}$ & Period	$0.1 \sim 1.0$ ($0.8 \sim 2.5$sec.)
Wave height	1cm, 2cm, $6 \sim 7$cm
θ	0^{o}, 30^{o}, 60^{o}, 90^{o}

The model that we use for evaluating the our numerical formulation is in Fig. 4.2 and Table 4.2. We discrete the body surface 30 elements in $\mathbf{e}_1$ direction and 6 elements in $\mathbf{e}_2$ direction, so total 180 elements and 217 nodes. Fig. 4.3 $\sim$ Fig. 4.14 show the results of the comparison and the vertical displacement of the numerical model. To easily figure out the vertical displacement, we divide it by the amplitude a of the incident wave. Fig. 4.3 $\sim$ Fig. 4.8 represent the results, as the frequency of the incident wave varies. Fig. 4.9 $\sim$ Fig. 4.14 is the results in oblique waves. As you can see in the figures, the results of our numerical formulation are in considerably agreement with the experiment.

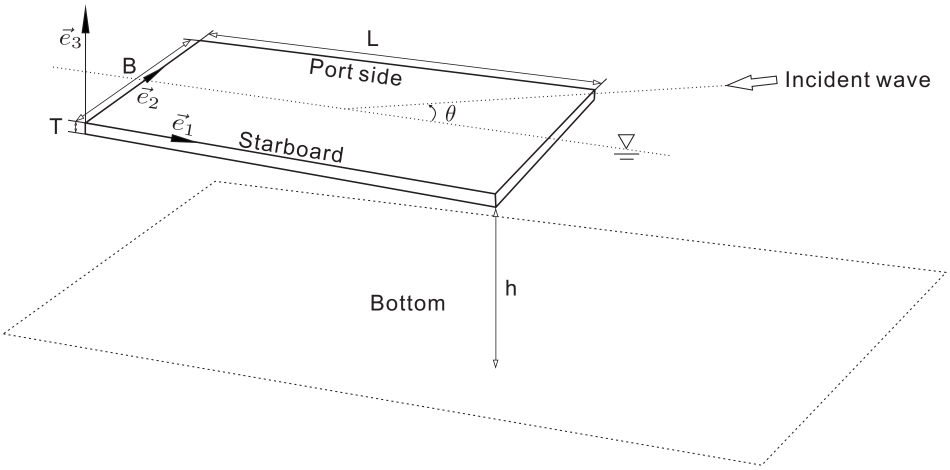

Figure 4.2: Schema of the numerical plate model

Table 4.2: The numerical plate model description

L	9.75m
B	1.95m
T	0.0545m
Stiffness (EI)	$1.788 \times 10^3 \mathrm{kgf \cdot m^2}$
Draft	0.0166m
Water Depth	1.9m
$\frac{\lambda}{\mathrm{L}}$	0.1, 0.5, 0.9
Wave height	1cm
θ	0° for $\frac{\lambda}{\mathrm{L}} = 0.1, 0.5$, and 0.9 $30^\circ, 60^\circ, 90^\circ$ for $\frac{\lambda}{\mathrm{L}} = 0.5$

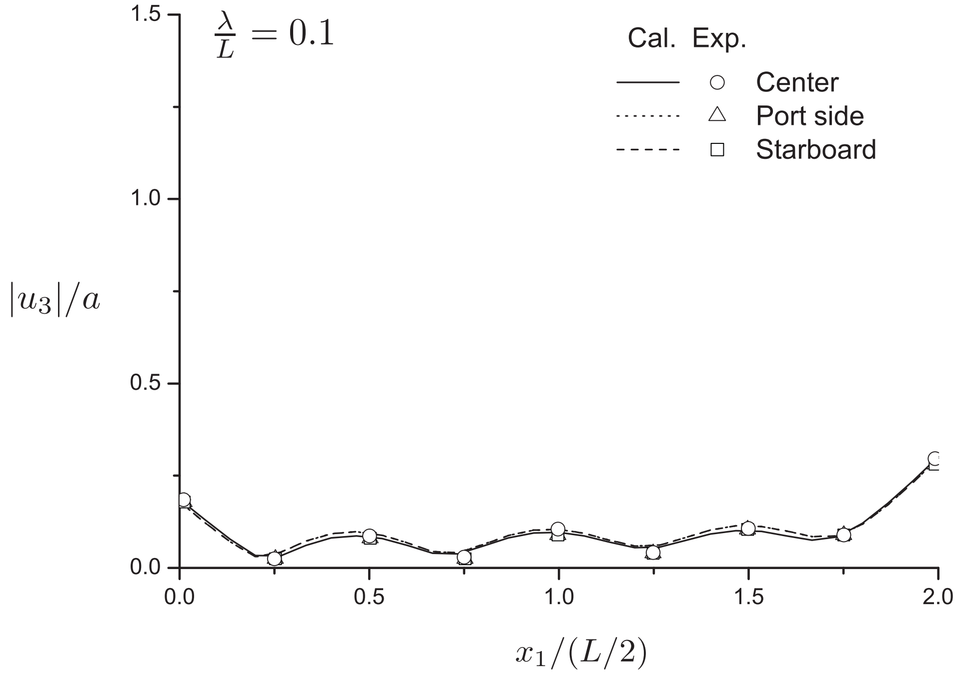

Figure 4.3: Comparison with the experiments, $\frac{\lambda}{L} = 0.1$, $\theta = 0^o$

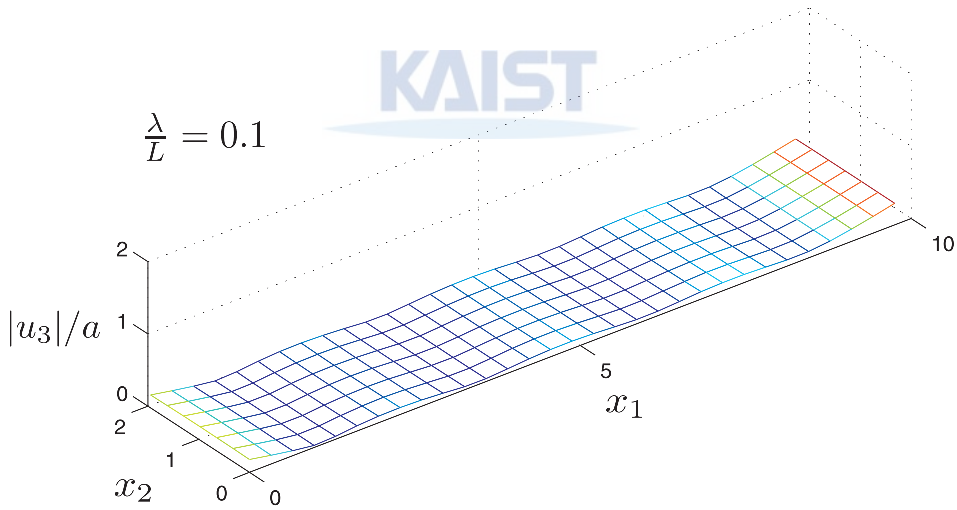

Figure 4.4: Vertical displacements of the numerical model, $\frac{\lambda}{L} = 0.1$, $\theta = 0^o$

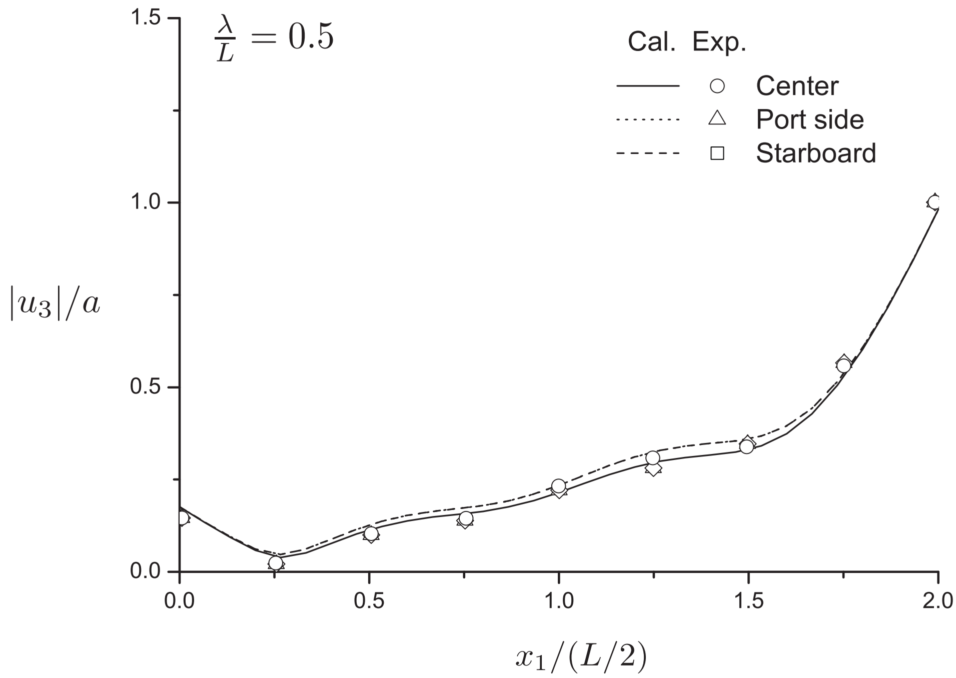

Figure 4.5: Comparison with the experiments, $\frac{\lambda}{\mathrm{L}} = 0.5$, $\theta = 0^{\mathrm{o}}$

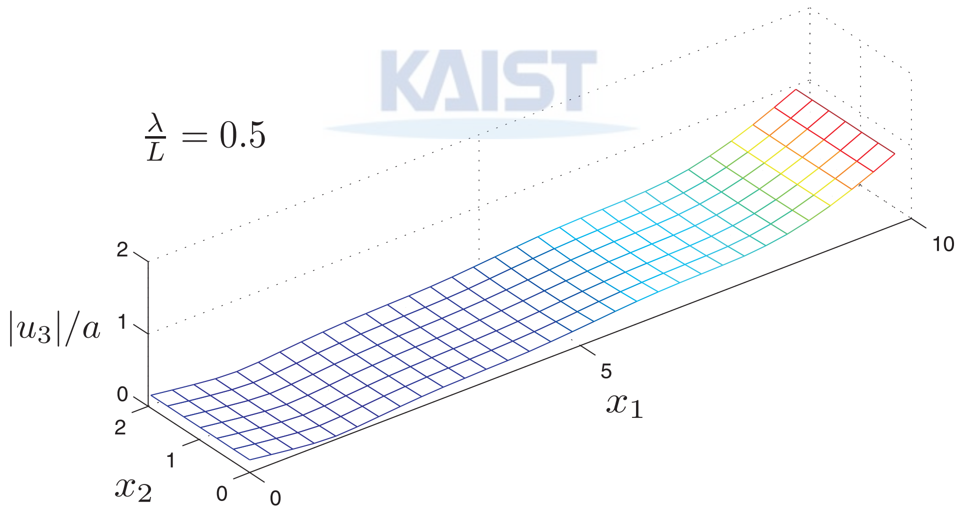

Figure 4.6: Vertical displacements of the numerical model, $\frac{\lambda}{\mathrm{L}} = 0.5$, $\theta = 0^{\mathrm{o}}$

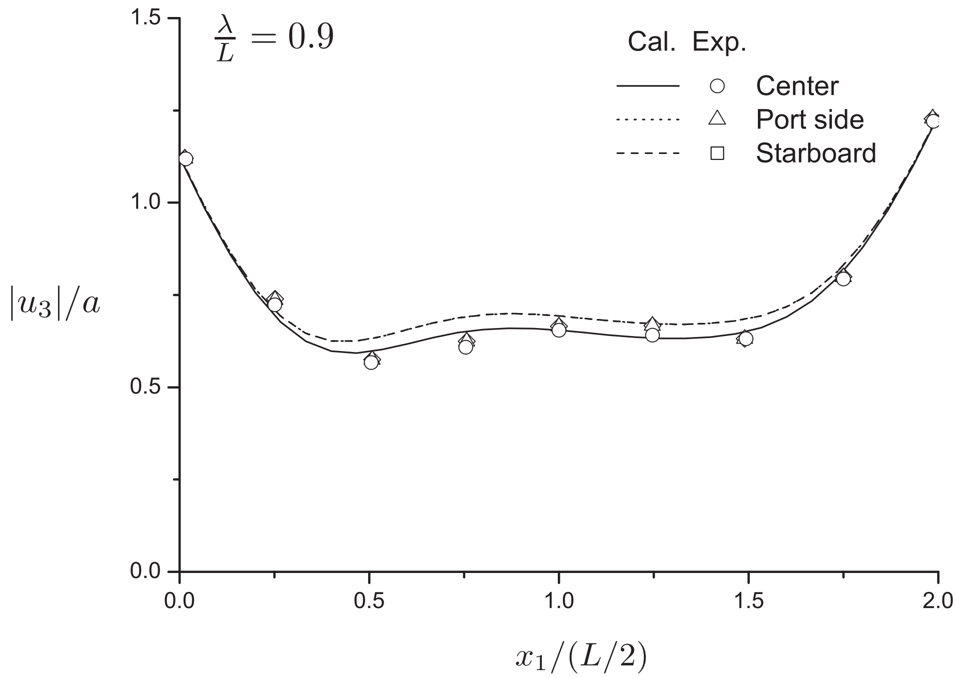

Figure 4.7: Comparison with the experiments, $\frac{\lambda}{\mathrm{L}} = 0.9$, $\theta = 0^{\mathrm{o}}$

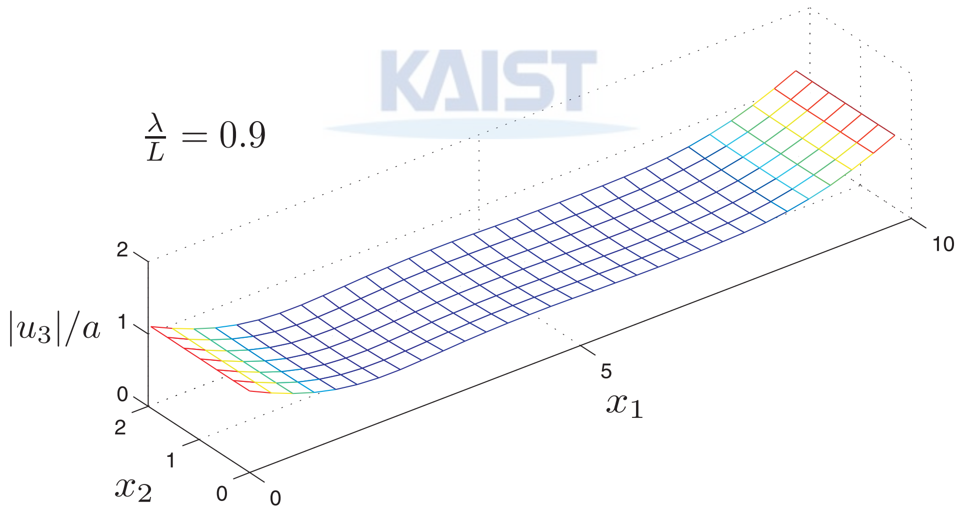

Figure 4.8: Vertical displacements of the numerical model, $\frac{\lambda}{\mathrm{L}} = 0.9$, $\theta = 0^{\mathrm{o}}$

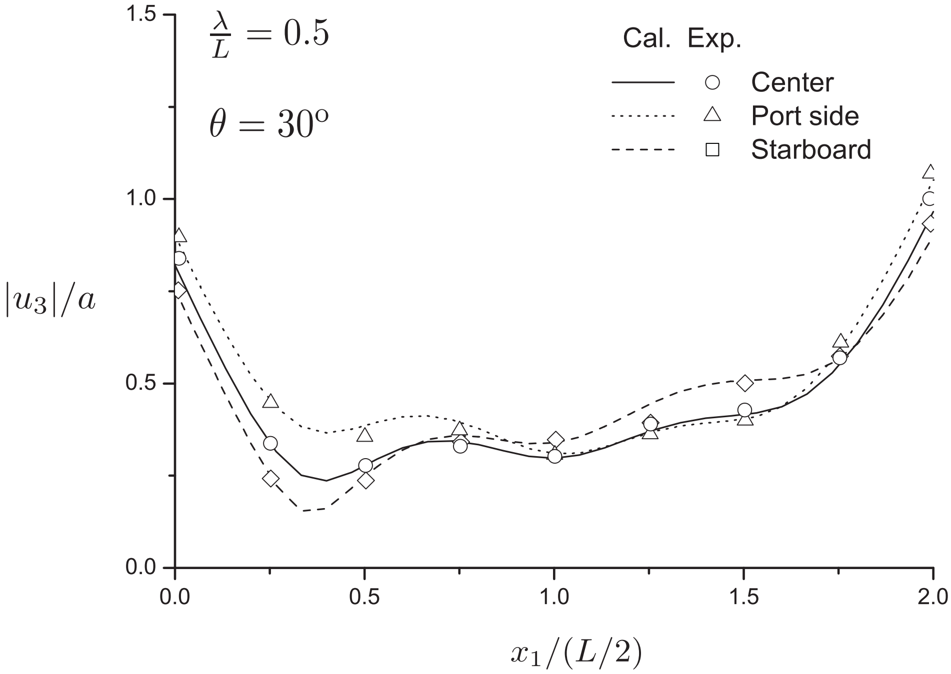

Figure 4.9: Comparison with the experiments, $\frac{\lambda}{\mathrm{L}} = 0.5$, $\theta = 30^{\rm o}$

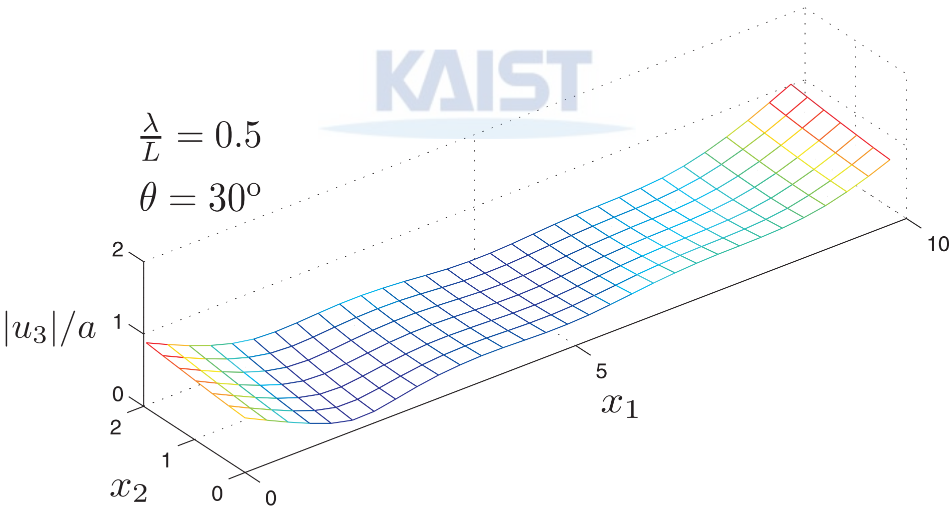

Figure 4.10: Vertical displacements of the numerical model, $\frac{\lambda}{\mathrm{L}} = 0.5$, $\theta = 30^{\rm o}$

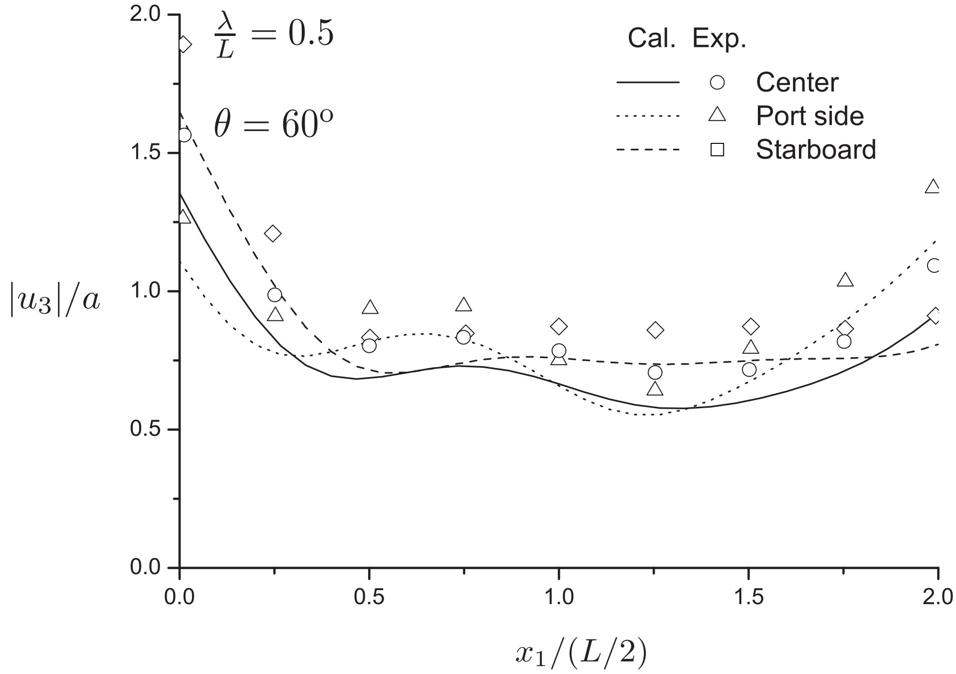

Figure 4.11: Comparison with the experiments, $\frac{\lambda}{L} = 0.5$, $\theta = 60^o$

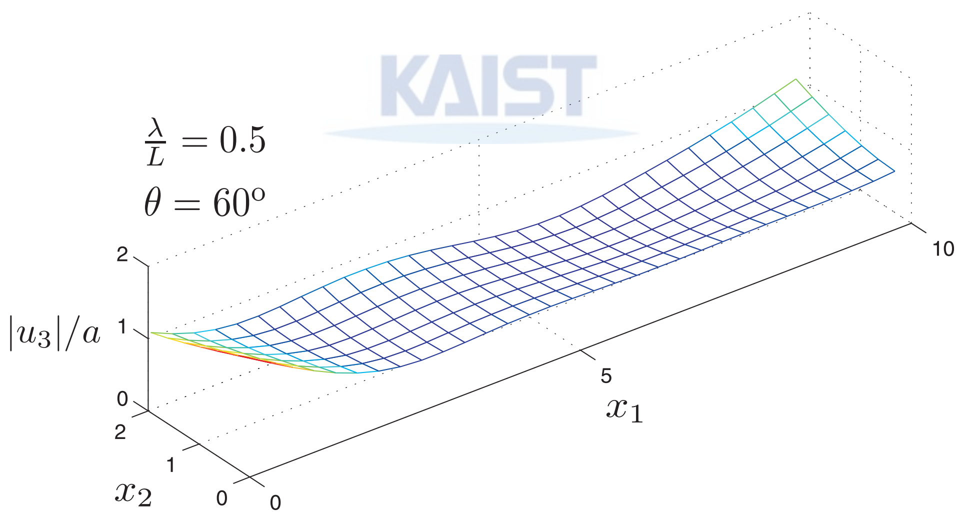

Figure 4.12: Vertical displacements of the numerical model, $\frac{\lambda}{L} = 0.5$, $\theta = 60^o$

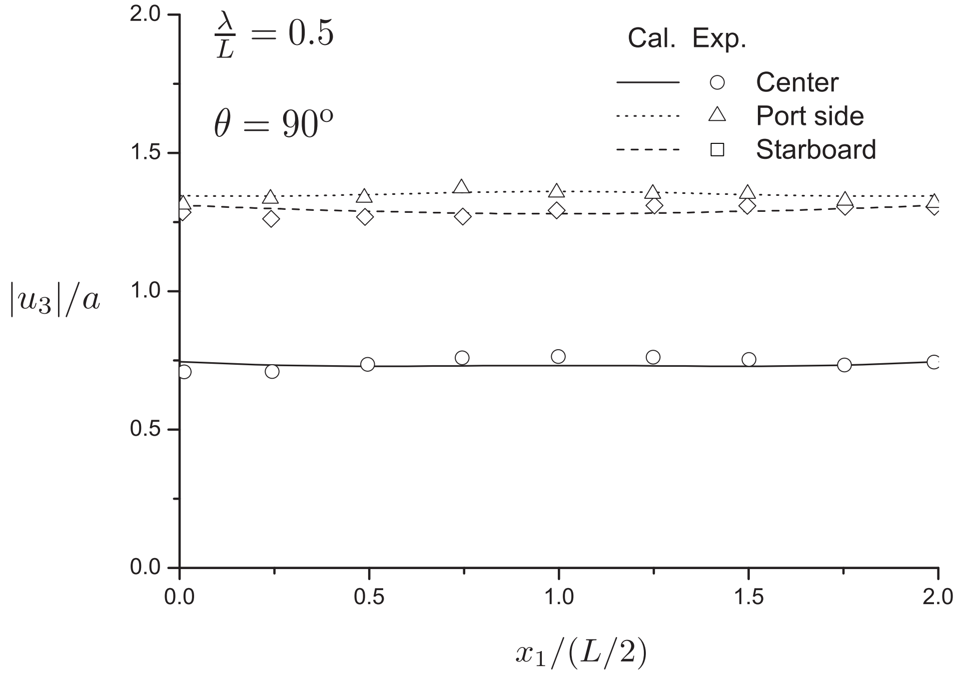

Figure 4.13: Comparison with the experiments, $\frac{\lambda}{L} = 0.5$, $\theta = 90^o$

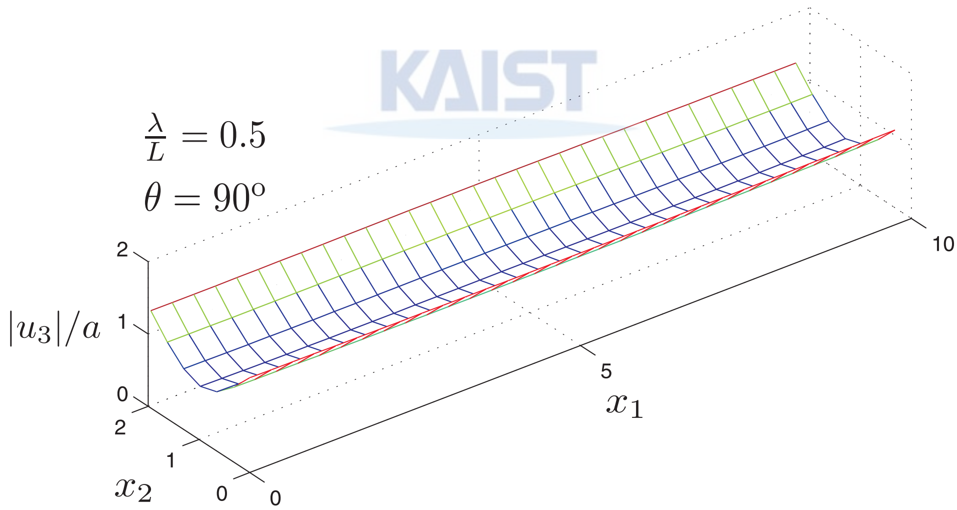

Figure 4.14: Vertical displacements of the numerical model, $\frac{\lambda}{L} = 0.5$, $\theta = 90^o$

4.2 A box-like model

We have computed our mathematical formulation using another numerical model, a box-like structure. You should be careful when assembling the total stiffness matrix and mass matrix for the structure at the node where two or three elements are jointed with a ridge angle, because the normal vector is different at this node according to elements. One of solutions to this problem is just using six degree of freedom at this node instead of five degree of freedom.

The numerical simulations have been performed using the model shown in the Fig. 4.15 and Table 4.3 . The discretization for this model is same with the plate model i.e., 180 elements with 217 nodes on the top and bottom surface, so total 504 elements with 506 nodes. We evaluate the displacements of the model as vary the incident angle. Fig. 4.16 $\sim$ Fig. 4.23 show the results of that. We represent the displacements of the model, which is divided by the incident wave amplitude, denoted a, on the top surface and bottom surface in each figures.

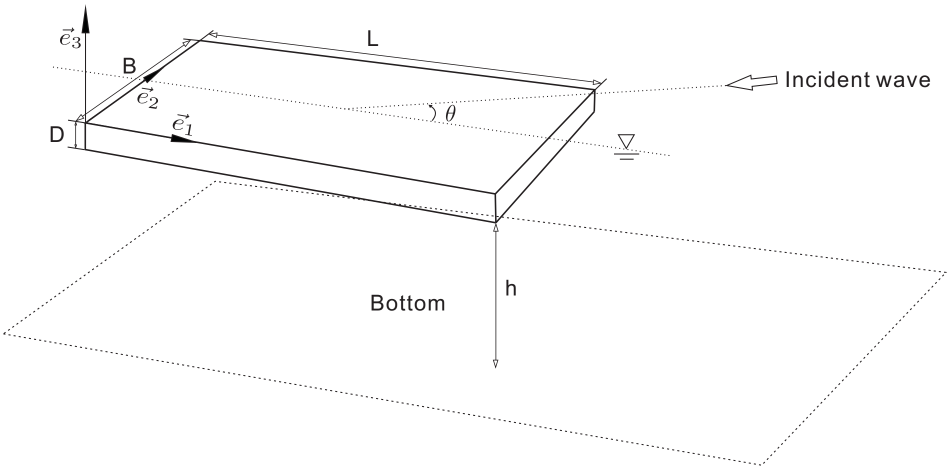

Figure 4.15: Schema of the numerical box-like models

Table 4.3: The numerical box-like model description

L	10m
B	2m
D	0.1m
E	$7 \times 10^8 \mathrm{N/m^2}$
Draft	0.05m
Water Depth	Infinite
$\frac{\lambda}{\mathrm{L}}$	0.5
θ	0^o, 30^o, 60^o, 90^o

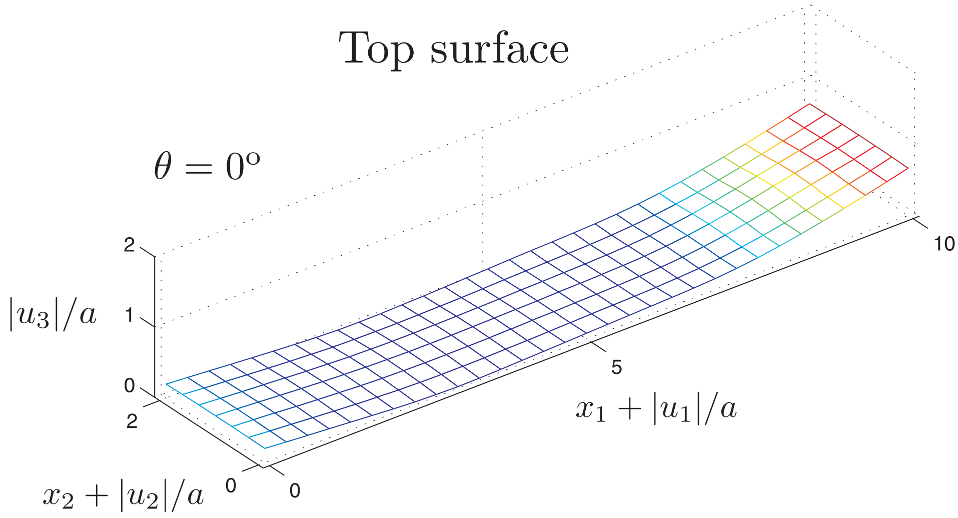

Figure 4.16: Displacements of the numerical box-like model (top surface), $\frac{\lambda}{L} = 0.5$, $\theta = 0^o$

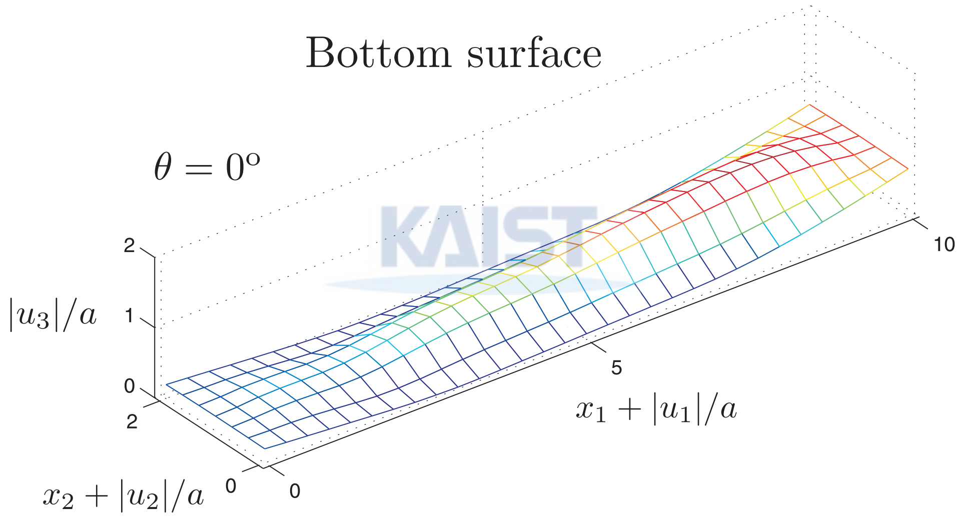

Figure 4.17: Displacements of the numerical box-like model (bottom surface), $\frac{\lambda}{L} = 0.5$, $\theta = 0^o$

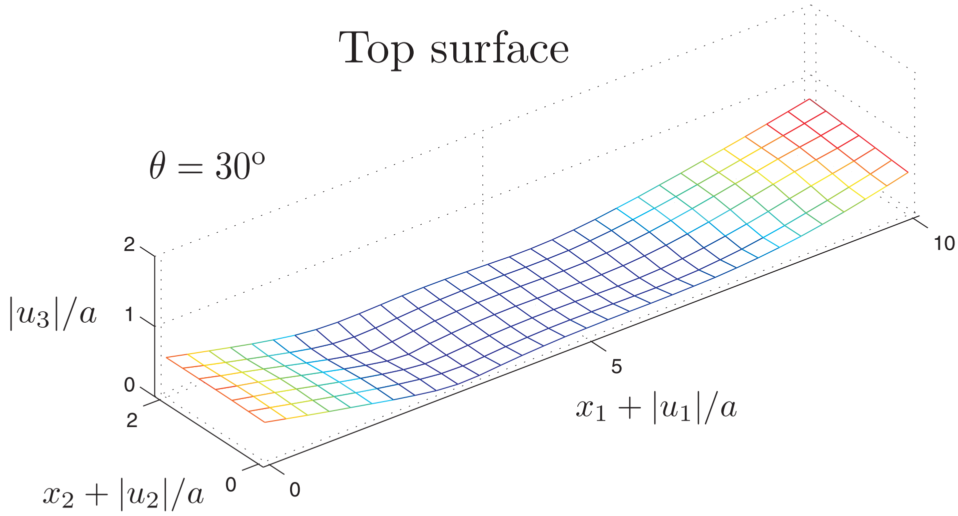

Figure 4.18: Displacements of the numerical box-like model (top surface), $\frac{\lambda}{\mathrm{L}} = 0.5$, $\theta = 30^{\mathrm{o}}$

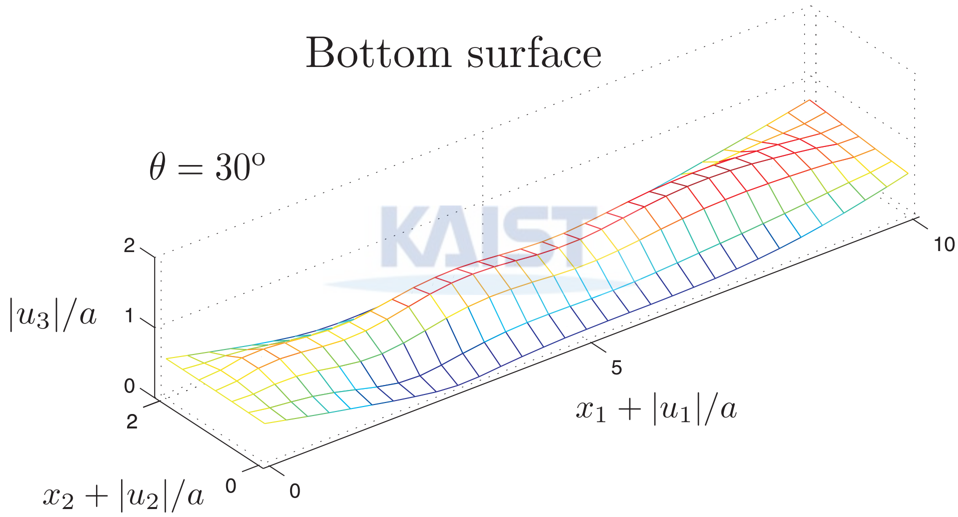

Figure 4.19: Displacements of the numerical box-like model (bottom surface), $\frac{\lambda}{\mathrm{L}} = 0.5$, $\theta = 30^{\mathrm{o}}$

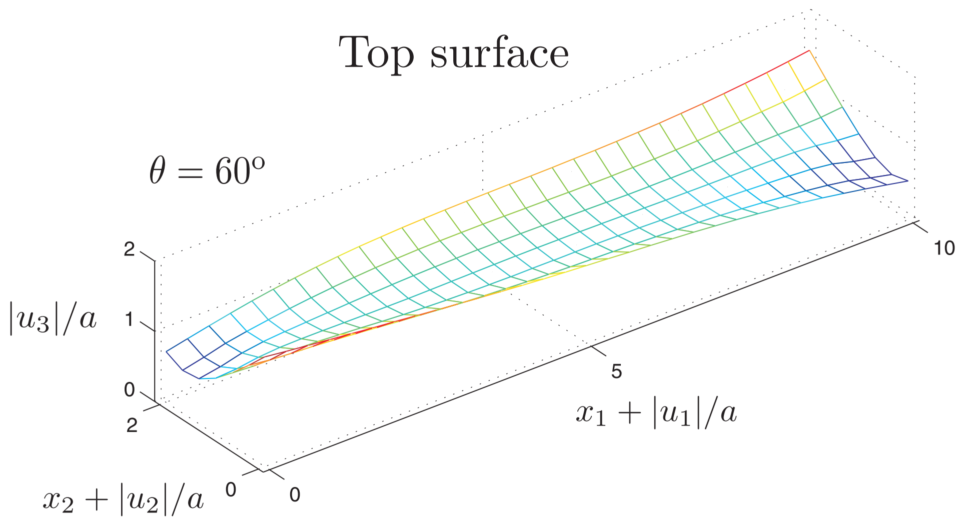

Figure 4.20: Displacements of the numerical box-like model (top surface), $\frac{\lambda}{\mathrm{L}} = 0.5$, $\theta = 60^{\mathrm{o}}$

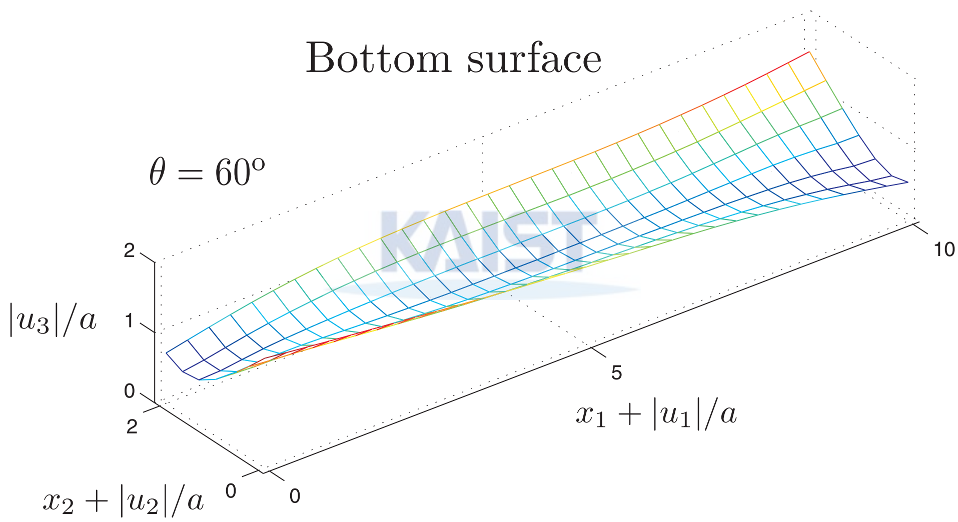

Figure 4.21: Displacements of the numerical box-like model (bottom surface), $\frac{\lambda}{\mathrm{L}} = 0.5$, $\theta = 60^{\mathrm{o}}$

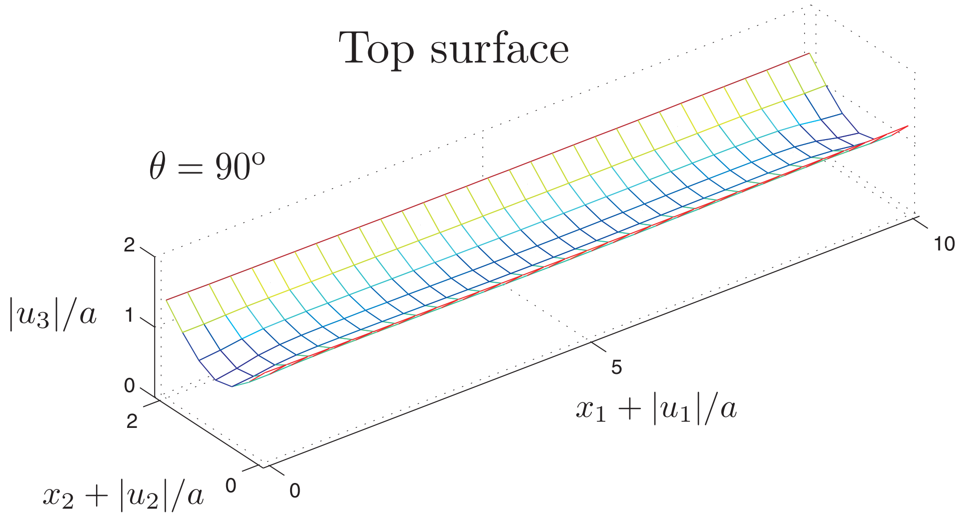

Figure 4.22: Displacements of the numerical box-like model (top surface), $\frac{\lambda}{L} = 0.5$, $\theta = 90^o$

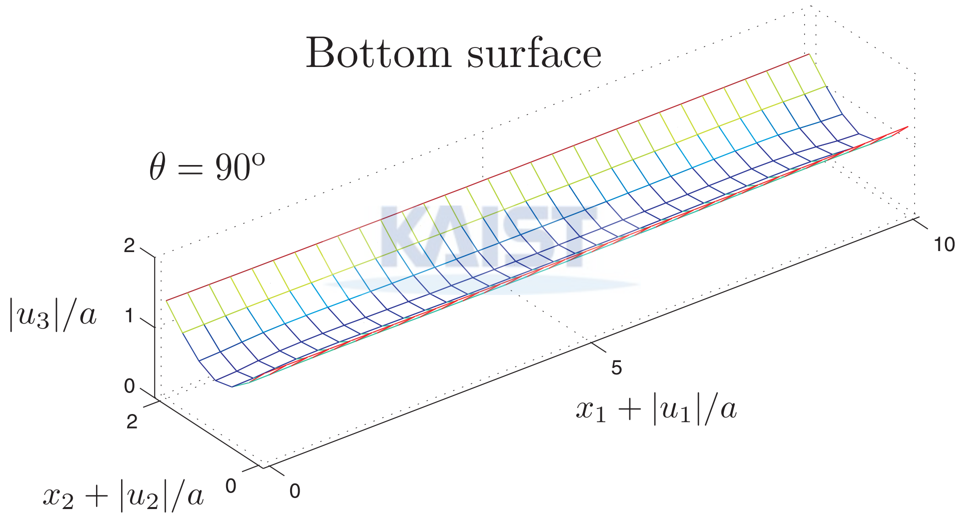

Figure 4.23: Displacements of the numerical box-like model (bottom surface), $\frac{\lambda}{L} = 0.5$, $\theta = 90^o$

4.3 A Wigley hull

To reflect three dimensional aspects of hydroelasticity, we studied a simple three dimensional ship-like structure, a Wigley hull. The Wigley hull has been tested frequently in ship research because of its simplicity. The geometry of the Wigley hull is defined by

$$x_2 = \frac{B}{2}\left(1 - \frac{4x_1^2}{L^2}\right)\left(1 - \frac{x_3^2}{d^2}\right) \tag{4.1}$$

where B is breadth, L is length, and d is draft. For comparison, we use same geometrical values and similar material properties with the model which has been tested already by Riggs H.R. *et al.*. [15]

The overall description of the numerical model is shown in the Fig. 4.24 and Table. 4.4. It is difficult to adjust our model to the model generated by Riggs H.R. *et al.*, because the finite shell model is different with it. The length, breadth, depth, draft, and Young's modulus are exactly same with it, but others are not. We set the thickness as physical one for the top deck and the side hull, but it wasn't. We set the density uniformly over the whole structure so that the draft would be half of the depth, but they had gave it only for the top deck. The total number of elements is 2800, 2780 of which are the four-node quadrilateral shell elements and 20 are three-node triangular shell elements. The number of quadrilateral and triangular elements is exactly same with his model, but we use the MITC3 and MITC4 shell elements to avoid the shear locking phenomenon. The overall meshes are shown in the Fig. 4.24 where a 10×100 mesh for the top deck and 9×100 meshes for the left and the right hulls respectively.

Fig. 4.25 and Fig. 4.26 represent the response amplitude operators for the displacement of bow, stern at middle of the top deck, and the center of the top deck respectively, where a means the incident wave amplitude and T means the it's period. We computed the model for the case that the wave period, T, is from 2 to 18 step by 2 and the incident angle θ is zero. As you can see in these figures, overall aspects are similar each other, but don't exactly same. This may be caused by the difference material properties and finite shell elements, as mentioned before.

We show the results for different incident angles. For a wave the length of which is half of the length of the model, Fig. 4.27 $\sim$ Fig. 4.42 show the displacements of the model. To easily see the displacements, we divided it by the amplitude of the incident wave and magnify that to ten times.

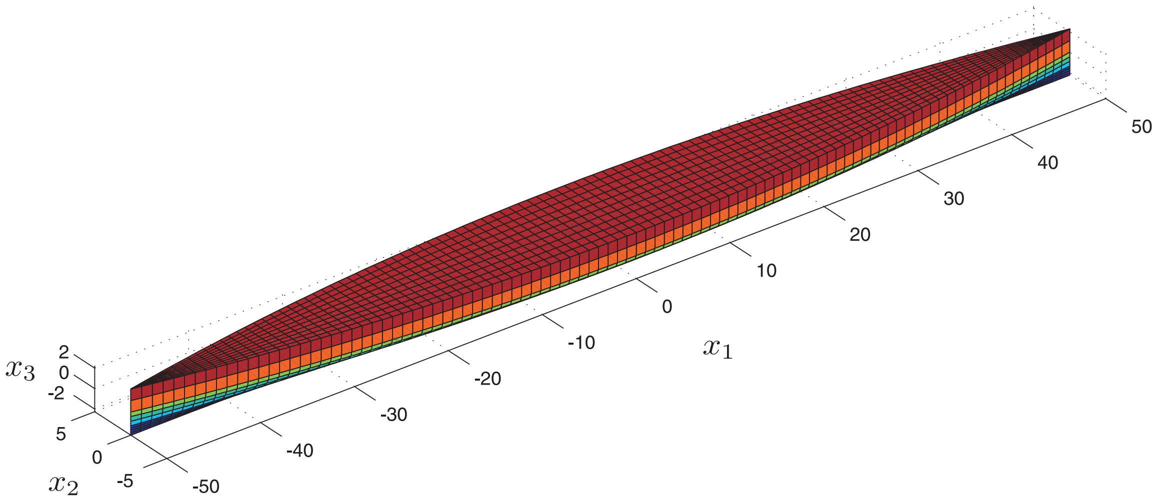

Figure 4.24: A Wigley hull model and it's meshes

Table 4.4: The numerical Wigley hull model description

Length (L)	100m
Breadth (B)	10m
Depth (D)	4.5m
Thickness (t)	0.25m for the top deck 0.15m for the side hull
Draft (d)	2.25m
Density (ρ)	$2.353 \times 10^3 \mathrm{kg/m^3}$
Young's modulus (E)	$7.5 \times 10^9 \mathrm{N/m^2}$
Water Depth	Infinite

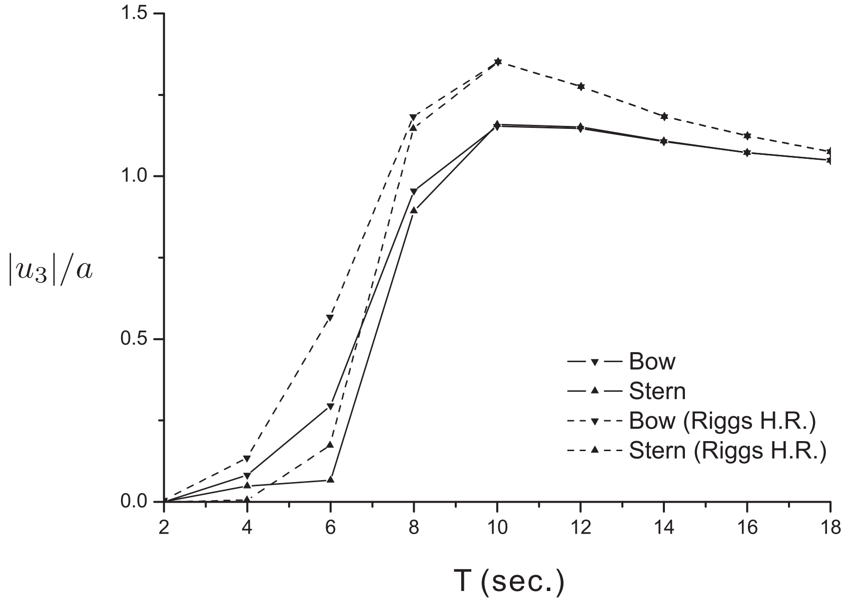

Figure 4.25: Vertical displacements of bow and stern at middle of the top deck (R.A.O.)

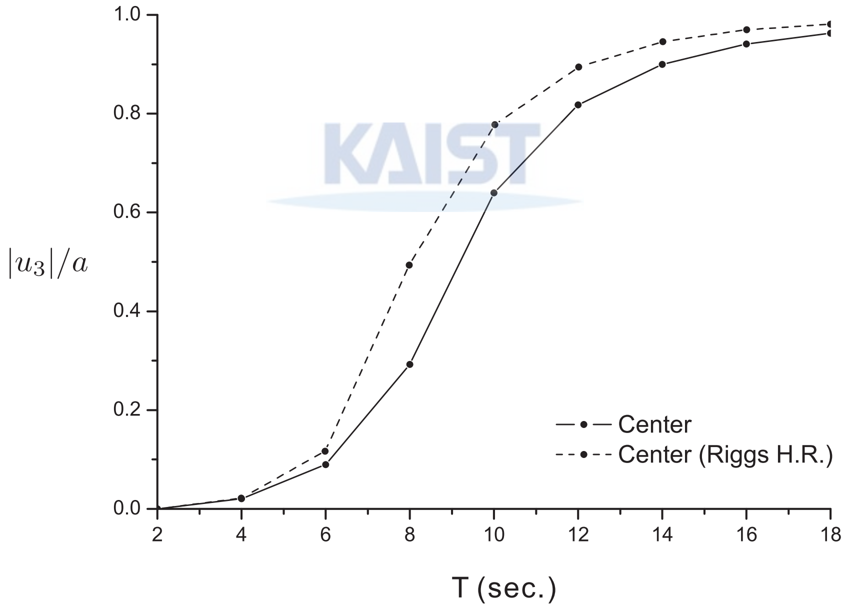

Figure 4.26: Vertical displacements of center of the top deck (R.A.O.)

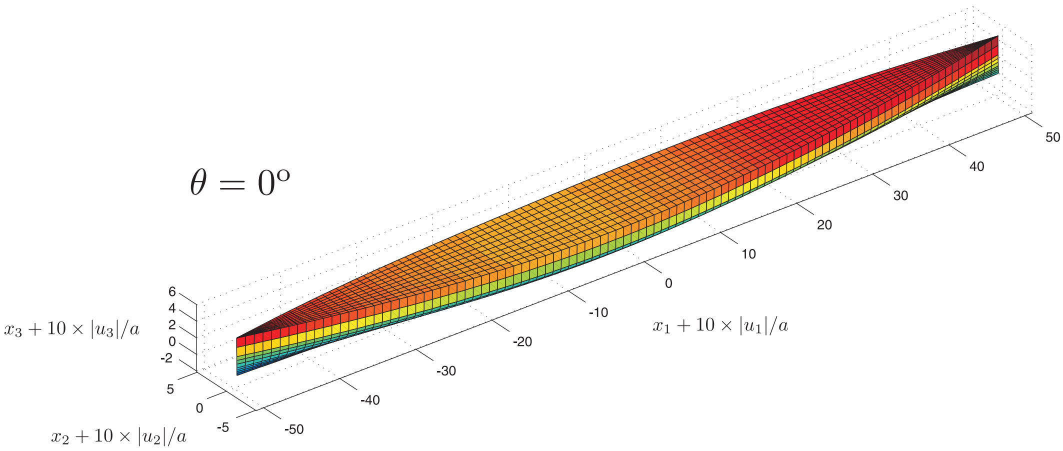

Figure 4.27: Displacements of the numerical Wigley hull model, overall, $\frac{\lambda}{\mathrm{L}} = 0.5$, $\theta = 0^{\mathrm{o}}$

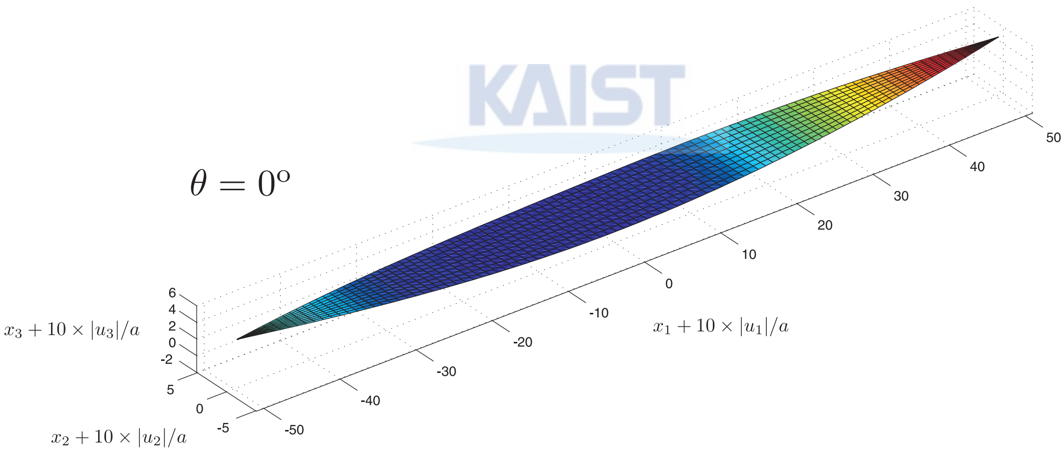

Figure 4.28: Displacements of the numerical Wigley hull model, the top deck, $\frac{\lambda}{\mathrm{L}} = 0.5$, $\theta = 0^{\mathrm{o}}$

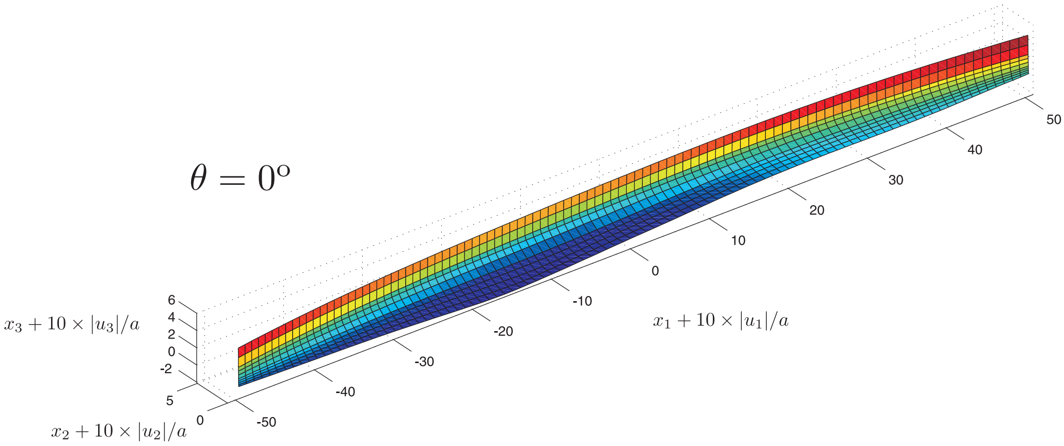

Figure 4.29: Displacements of the numerical Wigley hull model, the left hull, $\frac{\lambda}{\mathrm{L}} = 0.5$, $\theta = 0^o$

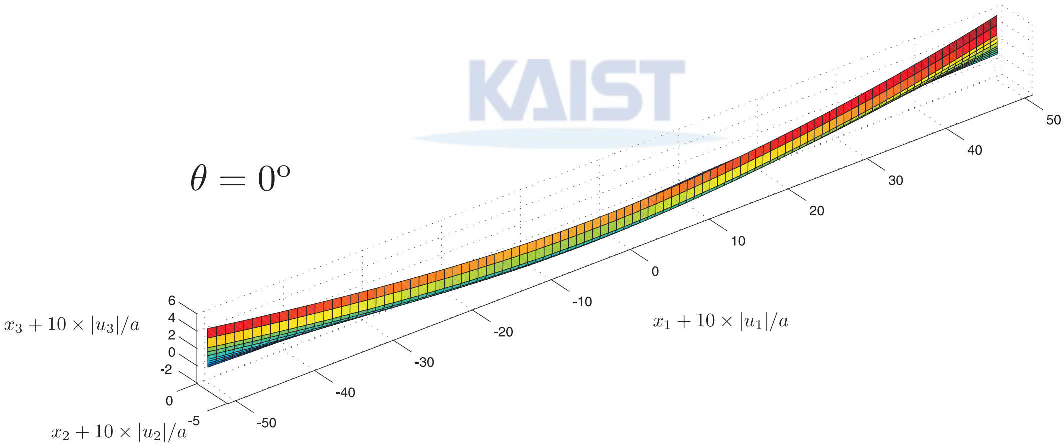

Figure 4.30: Displacements of the numerical Wigley hull model, the right hull, $\frac{\lambda}{\mathrm{L}} = 0.5$, $\theta = 0^o$

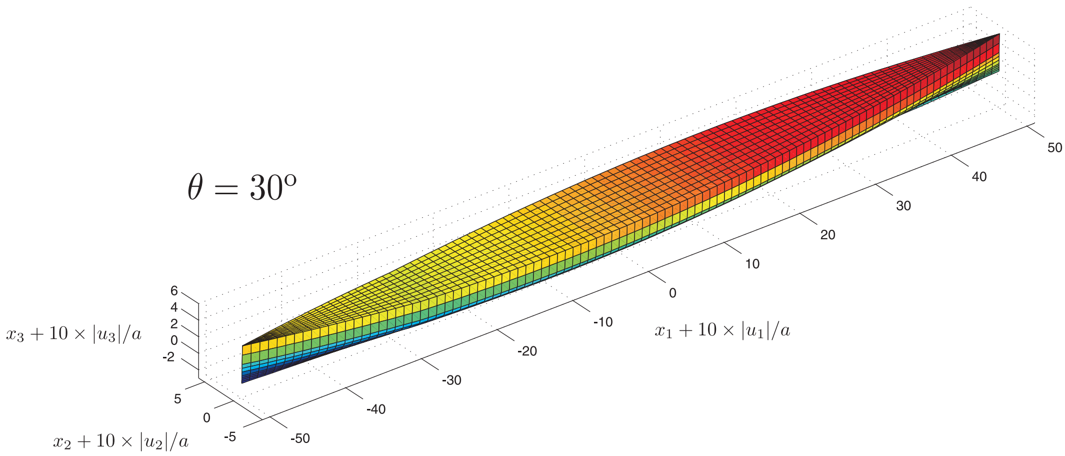

Figure 4.31: Displacements of the numerical Wigley hull model, overall, $\frac{\lambda}{\mathrm{L}} = 0.5$, $\theta = 30^{\mathrm{o}}$

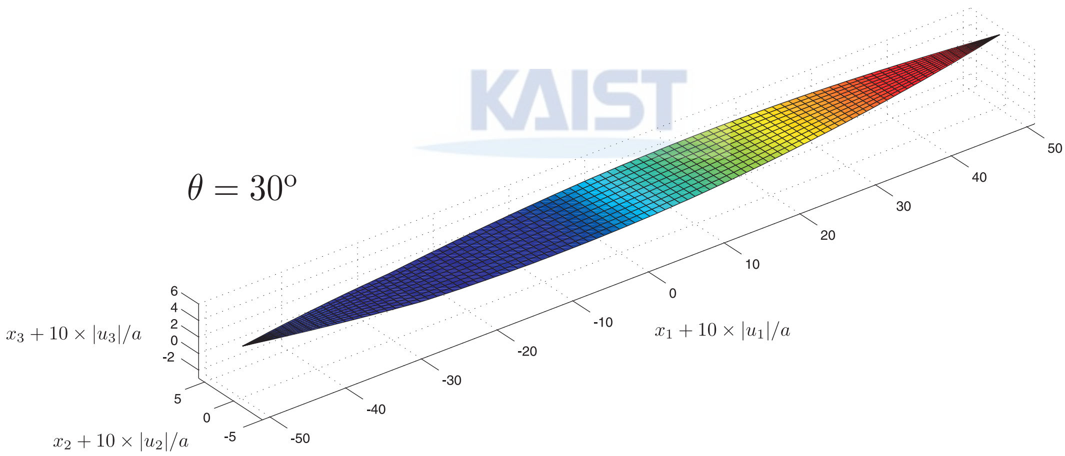

Figure 4.32: Displacements of the numerical Wigley hull model, the top deck, $\frac{\lambda}{\mathrm{L}} = 0.5$, $\theta = 30^{\mathrm{o}}$

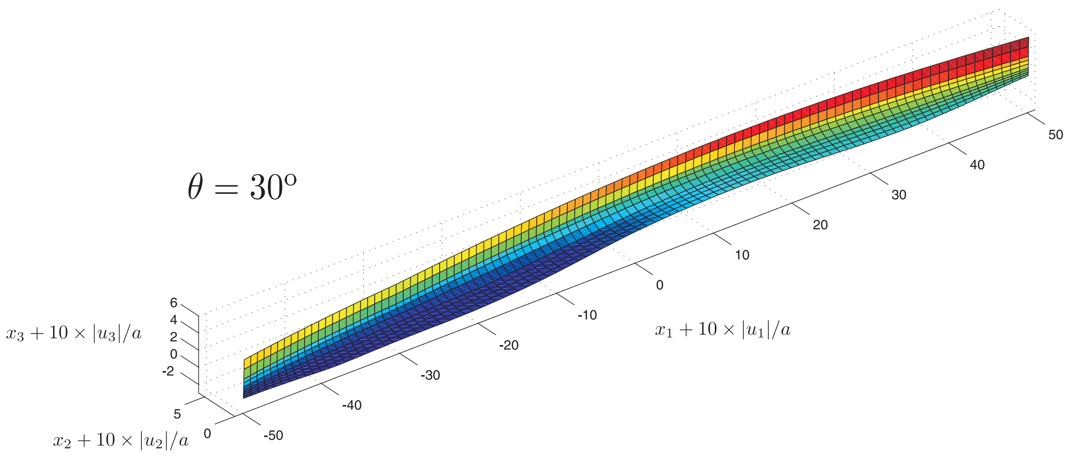

Figure 4.33: Displacements of the numerical Wigley hull model, the left hull, $\frac{\lambda}{\mathrm{L}} = 0.5$, $\theta = 30^{\rm o}$

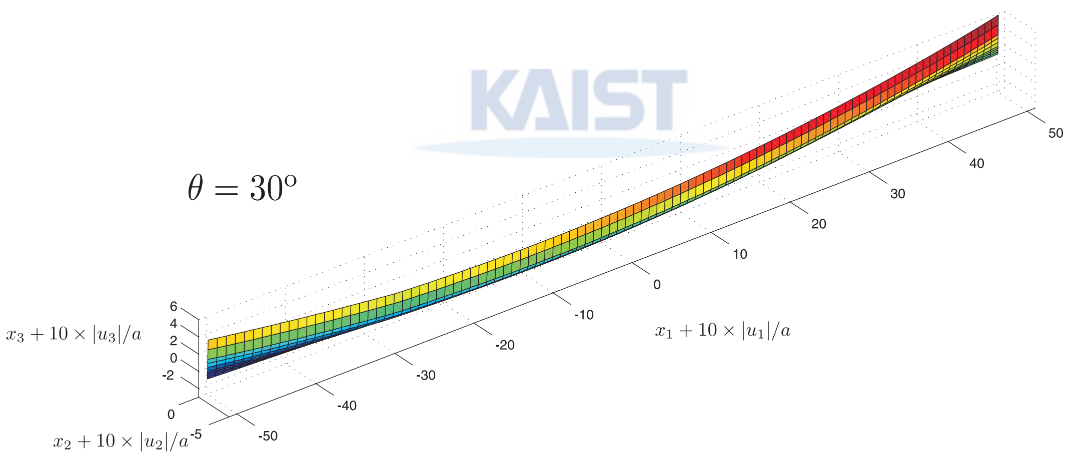

Figure 4.34: Displacements of the numerical Wigley hull model, the right hull, $\frac{\lambda}{\mathrm{L}} = 0.5$, $\theta = 30^{\rm o}$

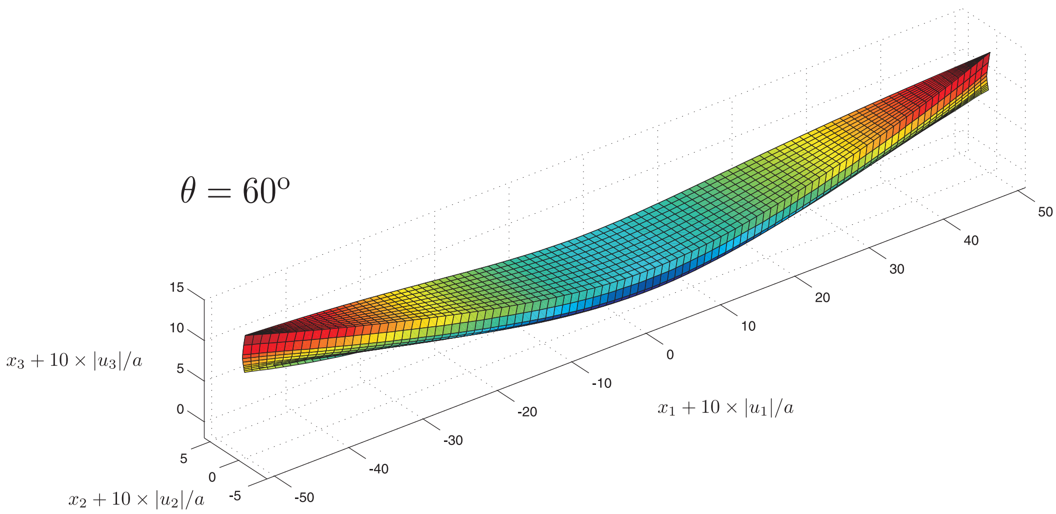

Figure 4.35: Displacements of the numerical Wigley hull model, overall, $\frac{\lambda}{\mathrm{L}} = 0.5$, $\theta = 60^{\mathrm{o}}$

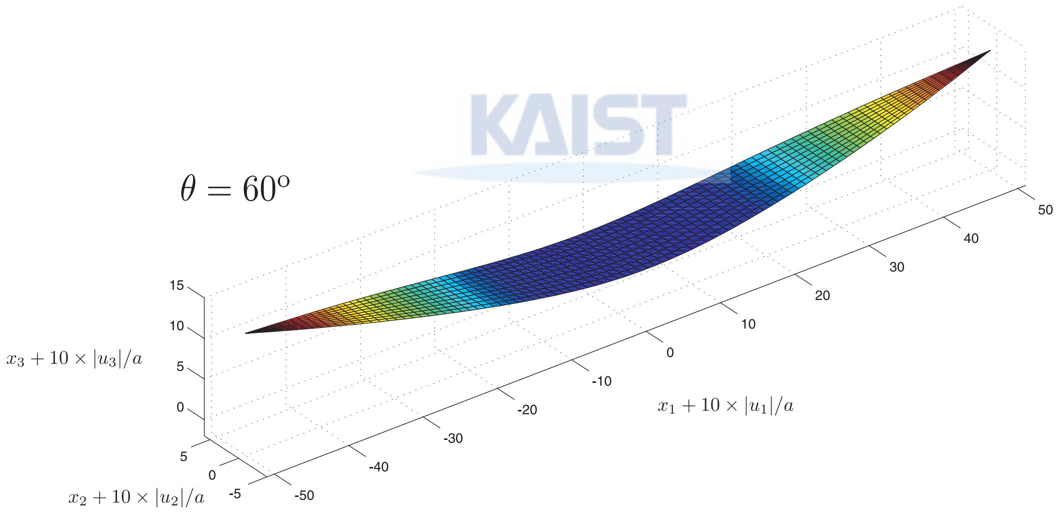

Figure 4.36: Displacements of the numerical Wigley hull model, the top deck, $\frac{\lambda}{\mathrm{L}} = 0.5$, $\theta = 60^{\mathrm{o}}$

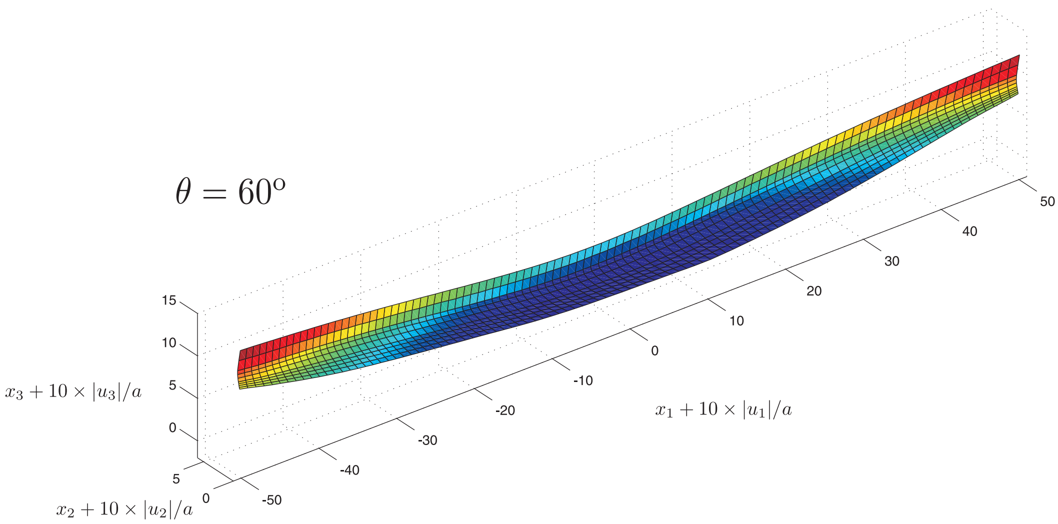

Figure 4.37: Displacements of the numerical Wigley hull model, the left hull, $\frac{\lambda}{\mathrm{L}} = 0.5$, $\theta = 60^{\rm o}$

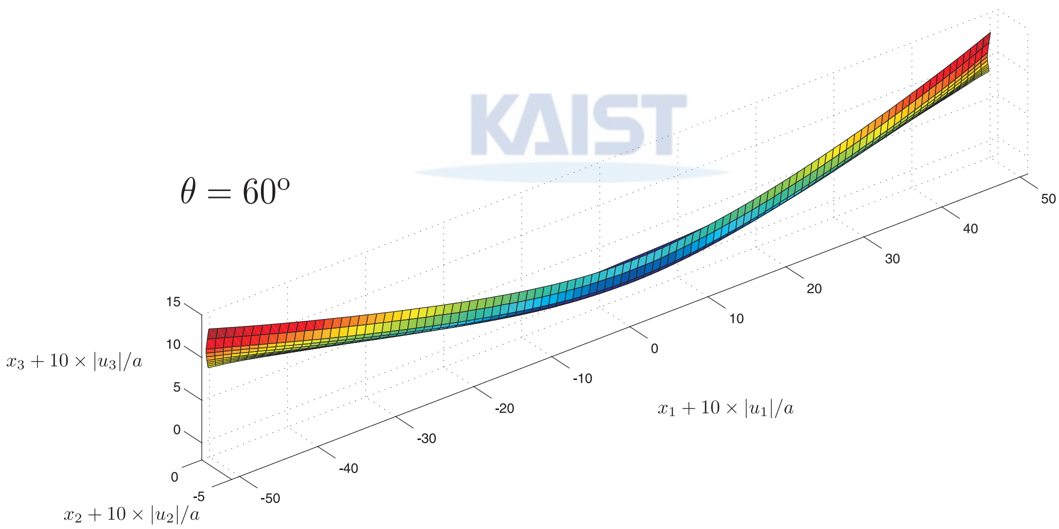

Figure 4.38: Displacements of the numerical Wigley hull model, the right hull, $\frac{\lambda}{\mathrm{L}} = 0.5$, $\theta = 60^{\rm o}$

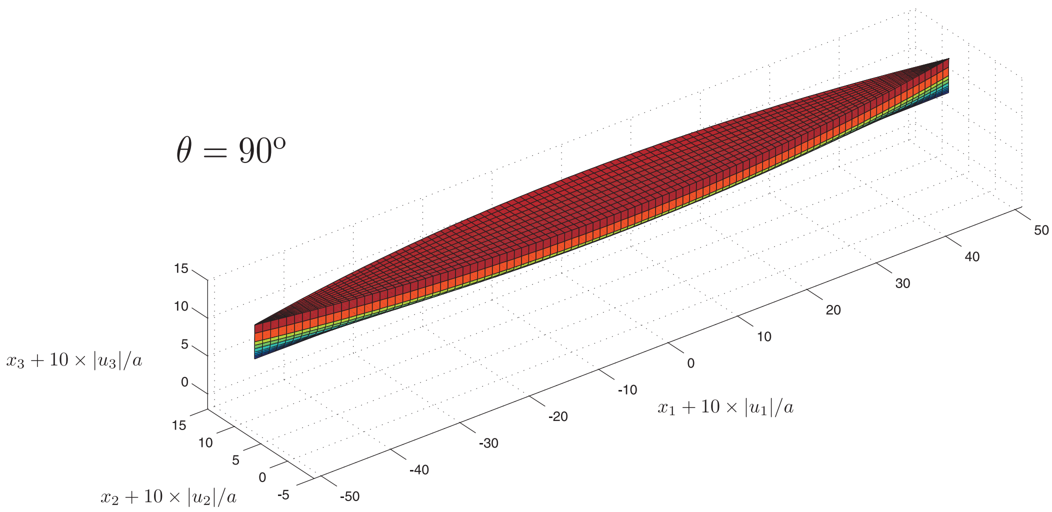

Figure 4.39: Displacements of the numerical Wigley hull model, overall, $\frac{\lambda}{\mathrm{L}} = 0.5$, $\theta = 90^{\mathrm{o}}$

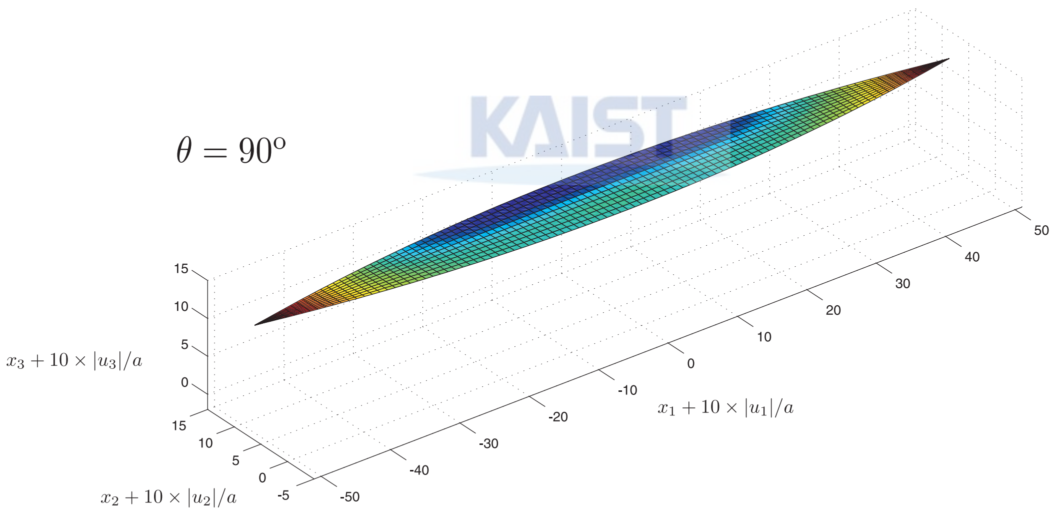

Figure 4.40: Displacements of the numerical Wigley hull model, the top deck, $\frac{\lambda}{\mathrm{L}} = 0.5$, $\theta = 90^{\mathrm{o}}$

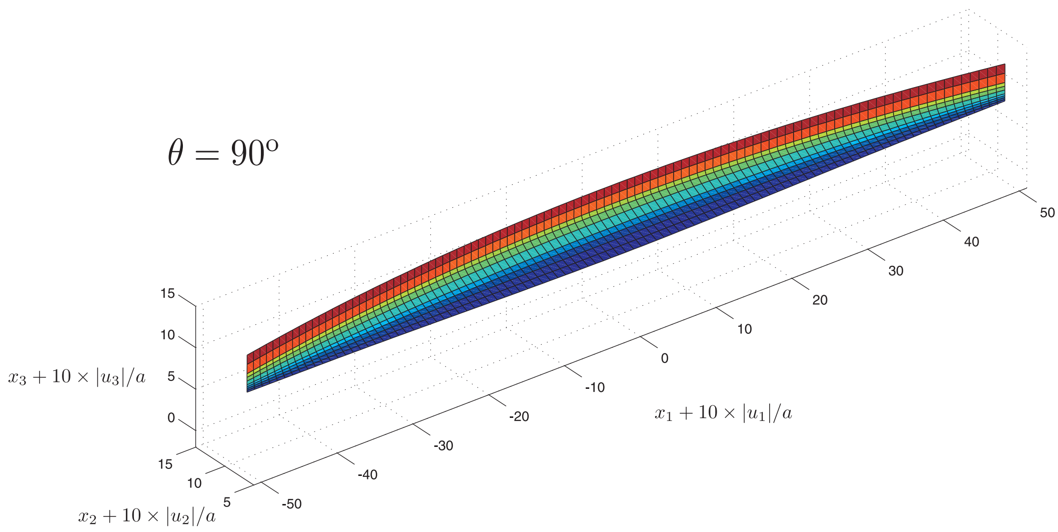

Figure 4.41: Displacements of the numerical Wigley hull model, the left hull, $\frac{\lambda}{\mathrm{L}} = 0.5$, $\theta = 90^{\mathrm{o}}$

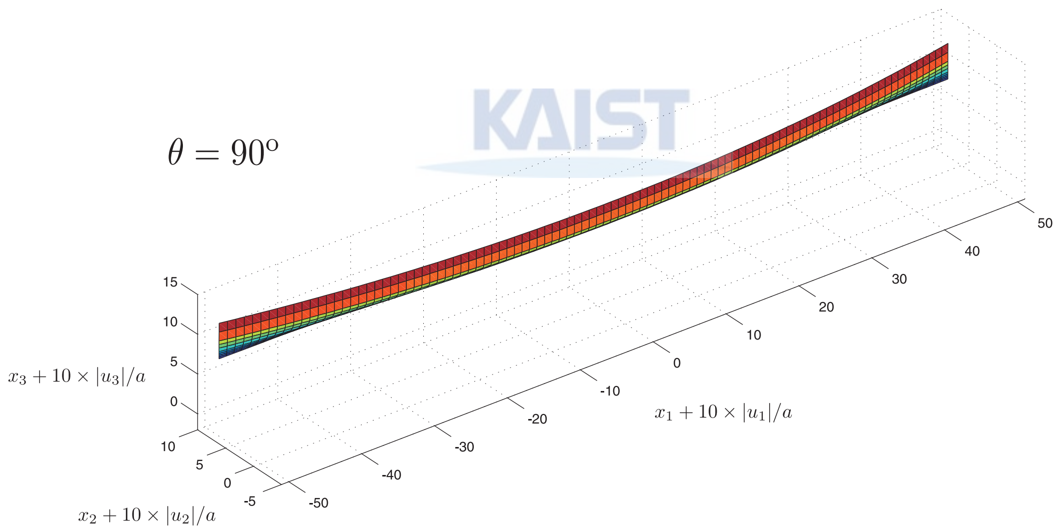

Figure 4.42: Displacements of the numerical Wigley hull model, the right hull, $\frac{\lambda}{\mathrm{L}} = 0.5$, $\theta = 90^{\mathrm{o}}$

Chapter 5. Conclusion

We have studied the three dimensional hydroelastic behavior of shell structures under regular waves. With appropriate assumptions, we derived the coupled equations for the general three dimensional hydroelastic analysis. To solve the coupled equations, we used the finite element method for the shell structure and boundary element method for the fluid. From comparison with the experiment results, we validated our mathematical formulation. To confirm the results related to three dimensional aspects of hydroelasticity, we simulated two additional models, one is the box-like model and another is the Wigley hull. In both cases, we have obtained satisfying results.

Appendices

Chapter A. The algorithm for the free surface Green's function

As mentioned before, the integral form of the free surface Green's function is highly complex and inefficient to evaluate. To overcome this problem, the Green's function has been studied a lot and very useful algorithm has been developed [1], [6], [10], [11], [12], [13], [14], [21]. That algorithms for infinite and finite depth cases are introduced in this chapter .

A.1 Infinite depth case

$$
\begin{aligned}
G &= \frac{1}{\sqrt{R^2 + (x_3 - \xi_3)^2}} + KF(X,Y) - 2\pi K e^{-Y} J_0(X) i \\
\frac{\partial G}{\partial R} &= -\frac{R}{(R^2 + (x_3 - \xi_3)^2)^{\frac{3}{2}}} - K^2 \Bigg(\frac{X}{(X^2 + Y^2)^{\frac{3}{2}}} - \pi e^{-Y} (H_1(X) + Y_1(X) - \frac{2}{\pi}) \\
&\quad + \frac{2e^{-Y}}{X} \int_0^Y \frac{te^t}{\sqrt{X^2 + t^2}}\,\mathrm{d}t - \frac{2Y}{X\sqrt{X^2 + Y^2}} \Bigg) + 2\pi K^2 e^{-Y} J_1(X) i \\
\frac{\partial G}{\partial \xi_3} &= -\frac{(\xi_3 - x_3)}{(R^2 + (x_3 - \xi_3)^2)^{\frac{3}{2}}} + K^2 \Bigg(\frac{1}{\sqrt{X^2 + Y^2}} + F + \frac{Y}{(X^2 + Y^2)^{\frac{3}{2}}} \Bigg) - 2\pi K^2 e^{-Y} J_0(X) i
\end{aligned}
$$

where

$$
\begin{aligned}
K &= \frac{\omega^2}{g} \\
R &= \sqrt{(x_1 - \xi_1)^2 + (x_2 - \xi_2)^2} \\
X &= KR \\
Y &= K \parallel x_3 + \xi_3 \parallel_2 \\
F(X,Y) &= P.V. \int_0^\infty \frac{\tau + 1}{\tau - 1} e^{-\tau Y} J_0(\tau X)\,\mathrm{d}\tau \\
&= \frac{1}{\sqrt{X^2 + Y^2}} - \pi e^{-Y} (H_0(X) + Y_0(X)) - 2 \int_0^Y \frac{e^{\,t - Y}}{\sqrt{X^2 + t^2}}\,\mathrm{d}t
\end{aligned}
$$

and J_n, Y_n and H_n are Bessel functions of the first, second kind and Struve function respectively (order n, $n = 0, 1$).

---

(1) In the domain, $8 < X$ and $20 < Y$

$$
\int_0^Y \frac{e^{\,t - Y}}{\sqrt{X^2 + t^2}}\,\mathrm{d}t = \sum_{n=0}^{\infty} n! P_n\left(\frac{Y}{\sqrt{X^2 + Y^2}}\right) \frac{1}{(X^2 + Y^2)^{\frac{1}{2}(n+1)}}
$$

where P_n is Legendre polynomial.

(2) In the domain, $X \leq \frac{1}{2}Y$

$$F(X,Y) = \frac{1}{\sqrt{X^2+Y^2}} + 2\sum_{n=0}^{\infty} \frac{(-X^2/4)^n}{(n!)^2}\Big(\sum_{m=1}^{2n} \frac{(m-1)!}{Y^m} - e^{-Y}Ei(Y)\Big)$$

where $Ei(Y)$ is exponential integral.

(3) In the domain, $3.7 < X$ and $4Y \leq X$

$$\int_0^Y \frac{e^{\,t-Y}}{\sqrt{X^2+t^2}}\,\mathrm{dt} = \frac{1}{X}\left(I_0(Y) + \sum_{n=1}^{N}(-1)^n \frac{X^{-2n}}{n!}\frac{(2n-1)!!}{2^n} I_{2n}(Y)\right)$$

where

$$I_0 = 1 - e^{-Y}$$
$$I_{2n} = Y^{2n} - 2nY^{2n-1} + 2n(2n-1)I_{2n-2}$$

(4) In the domain, $Y \leq 2$ and the rest of X except the above region

$$F(X,Y) = \frac{1}{\sqrt{X^2+Y^2}} - 2e^{-Y}\Bigg(J_0(X)\ln\Big(\frac{Y}{X} + \sqrt{1+\frac{Y^2}{X^2}}\Big) + \frac{\pi}{2}Y_0(X) + \frac{\pi}{2X}H_0(X)\sqrt{X^2+Y^2} + \sqrt{X^2+Y^2}\sum_{m=0}^{\infty}\sum_{n=1}^{\infty} C_{mn}X^{2m}Y^n\Bigg)$$

where

$$C_{0n} = \frac{1}{(n+1)(n+1)!}$$
$$C_{mn} = -\Big(\frac{n+2}{n+1}\Big)C_{m-1,n+2}$$

(5) In the rest domain, $2 < Y < 20$

$$\int_0^Y \frac{e^{\,t-Y}}{\sqrt{X^2+t^2}}\,\mathrm{dt} = \frac{1}{X^2+Y^2} - \frac{e^{-Y}}{X} + \frac{Y}{(X^2+Y^2)^{\frac{3}{2}}}R(X,Y)$$
$$e^{-Y}\int_0^Y \frac{te^t}{\sqrt{X^2+t^2}}\,\mathrm{dt} = \frac{Y-1}{\sqrt{X^2+t^2}} + \frac{e^{-Y}}{X} + \frac{Y(Y-2)}{(X^2+Y^2)^{\frac{3}{2}}}Rx(X,Y)$$

or

$$e^{-Y}\int_0^Y \frac{te^t}{\sqrt{X^2+t^2}}\,\mathrm{dt} = \frac{Y-1}{\sqrt{X^2+t^2}} + \frac{e^{-Y}}{X} + \frac{Y(Y-1)}{(X^2+Y^2)^{\frac{3}{2}}}Rx'(X,Y)$$

where $R(X,Y)$ and $Rx(X,Y)$ (or $Rx'(X,Y)$) are some slowly-varying functions, and could be approximated by double Chebyshev expansions.

A.2 Finite depth case

$$
\begin{aligned}
G = & \frac{1}{\sqrt{R^2+(x_3-\xi_3)^2}} + \frac{1}{\sqrt{R^2+(2h+x_3+\xi_3)^2}} \\
& + 2\int_0^\infty \frac{(k+K)\cosh k(x_3+h)\cosh k(\xi_3+h)}{k\sinh kh - K\cosh kh} e^{-kh} J_0(kR)\,\mathrm{d}k \\
& + 2\pi \frac{K^2-k_0^2}{k_0^2 h - K^2 h + K} \cosh k_0(x_3+h)\cosh k_0(\xi_3+h) J_0(k_0 R) i
\end{aligned}
$$

where h is the water depth, and k_0 is positive real root of the dispersion relation.

---

(1) In the domain, $\frac{1}{2} < \frac{R}{h}$

$$
\begin{aligned}
G = & 2\pi \frac{K^2-k_0^2}{k_0^2 h - K^2 h + K} \cosh k_0(x_3+h)\cosh k_0(\xi_3+h)[Y_0(k_0R)+iJ_0(k_0R)] \\
& + 4\sum_{n=1}^{\infty} \frac{k_n^2+K^2}{k_n^2 h + K^2 h - K} \cos k_n(x_3+h)\cos k_n(\xi_3+h) K_0(k_n R) \\
\frac{\partial G}{\partial R} = & 2\pi \frac{K^2-k_0^2}{k_0^2 h - K^2 h + K} \cosh k_0(x_3+h)\cosh k_0(\xi_3+h)[-k_0 Y_1(k_0R) - ik_0 J_1(k_0R)] \\
& - 4\sum_{n=1}^{\infty} \frac{k_n^2+K^2}{k_n^2 h + K^2 h - K} \cos k_n(x_3+h)\cos k_n(\xi_3+h) k_n K_1(k_n R) \\
\frac{\partial G}{\partial \xi_3} = & 2\pi \frac{K^2-k_0^2}{k_0^2 h - K^2 h + K} k_0 \cosh k_0(x_3+h)\sinh k_0(\xi_3+h)[Y_0(k_0R)+iJ_0(k_0R)] \\
& - 4\sum_{n=1}^{\infty} \frac{k_n^2+K^2}{k_n^2 h + K^2 h - K} k_n \cos k_n(x_3+h)\sin k_n(\xi_3+h) K_0(k_n R)
\end{aligned}
$$

where K_n is modified Bessel function of the second kind (order n, $n = 0, 1$), and k_n is positive pure imaginary roots of the dispersion relation multiplied by $-i$ ($n = 1, 2, \cdots$).

(2) In the domain, $\frac{R}{h} \leq \frac{1}{2}$

$$
\begin{aligned}
Re(G) &= KL(X, |Y-Z|, H) + KL(X, 2H-Y-Z, H) \\
Re(\frac{\partial G}{\partial R}) &= K^2 \frac{\partial L}{\partial X}\Big|_{(X,|Y-Z|,H)} + K^2 \frac{\partial L}{\partial X}\Big|_{(X,2H-Y-Z,H)} \\
Re(\frac{\partial G}{\partial \xi_3}) &= K^2 \frac{\partial L}{\partial V}\Big|_{(X,(Y-Z),H)} + K^2 \frac{\partial L}{\partial V}\Big|_{(X,2H-Y-Z,H)} \quad \text{for} \quad Y-Z \geq 0 \\
&= -K^2 \frac{\partial L}{\partial V}\Big|_{(X,(Z-Y),H)} + K^2 \frac{\partial L}{\partial V}\Big|_{(X,2H-Y-Z,H)} \quad \text{for} \quad Y-Z < 0
\end{aligned}
$$

where the auxiliary function L is defined by

$$L = \frac{1}{(X^2+V^2)^{\frac{1}{2}}} + P.V.\int_0^\infty \frac{(k+1)\cosh kV}{k\sinh kH - \cosh kH} e^{-kH} J_0(kX)\,\mathrm{d}k$$
$$= \frac{1}{(X^2+V^2)^{\frac{1}{2}}} + F(X, 2H-V) + F(X, 2H+V)$$
$$+ P.V.\int_0^\infty \left(\frac{1}{k\sinh kH - \cosh kH} - \frac{2e^{-kH}}{k-1}\right)(k+1)\cosh kV e^{-kH} J_0(kX)\,\mathrm{d}k$$

where

$$X = KR, \quad Y = K|x_3|, \quad Z = K|\xi_3|, \quad H = Kh$$

The integral in the above equation L could be approximated by Chebyshev expansions, because we can evaluate it by using contour integration. One example of contour to evaluate the integral in the equation L is shown in the Fig. A.1.

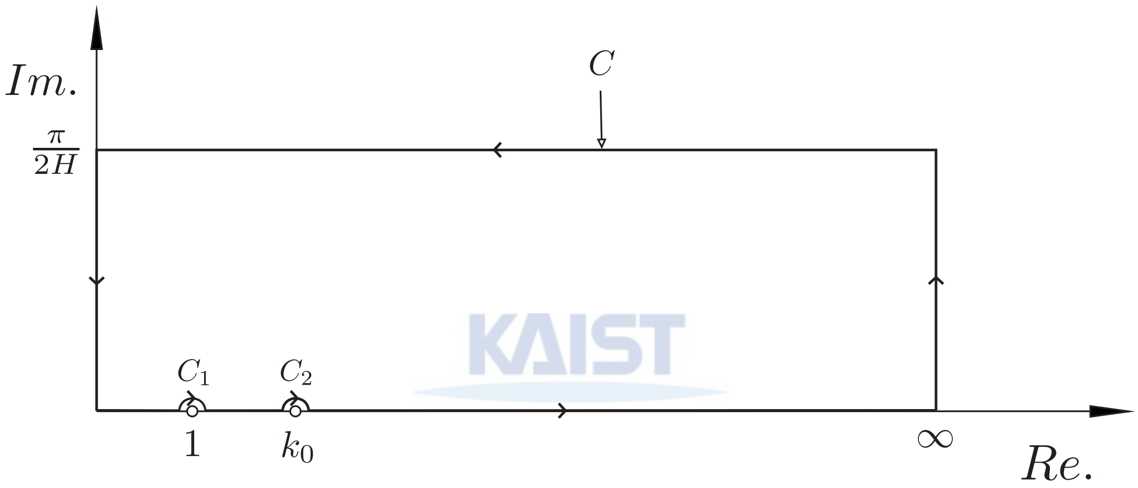

Figure A.1: One example of contour for the integral in the equation L

If we define like

$$f(k) = \left(\frac{1}{k\sinh kH - \cosh kH} - \frac{2e^{-kH}}{k-1}\right)(k+1)\cosh kV e^{-kH} J_0(kX)$$

then from Cauchy's integral theorem

$$\oint_C f(z)\,\mathrm{d}z = 0, \quad z = x + yi$$

where x is real component and y is image component of complex variable z. So, with residue integration method we can compute the integral in the equation L like

$$P.V.\int_0^\infty f(k)\,\mathrm{d}k$$
$$= -\int_{C_1} f(z)\,\mathrm{d}z - \int_{C_2} f(z)\,\mathrm{d}z - \int_0^{\frac{\pi}{2H}} f(y)\Big|_{x=\infty}\mathrm{d}y - \int_\infty^0 f(x)\Big|_{y=\frac{\pi}{2H}}\mathrm{d}x - \int_{\frac{\pi}{2H}}^0 f(y)\Big|_{x=0}\mathrm{d}y$$

where

$$\int_{C_1} f(z)\,\mathrm{d}z = -\pi i\,\mathrm{Res}\,[f(z), z=1]$$
$$\int_{C_2} f(z)\,\mathrm{d}z = -\pi i\,\mathrm{Res}\,[f(z), z=k_0]$$

Chapter B. Special cases

When the body surface, S_B, is at $x_3 = 0$, i.e. very thin plate or beam cases, we can modify the coupled equations, (2.50) and (2.51), more efficiently. In these cases, the final equations are coupled by the displacements of the structure and the total pressure of the fluid.

B.1 The plate case

Consider the right side of the equations (2.35). As we mentioned before, the coefficient -2π comes from the integration of the source component of the Green's function over very small surface. In general case, as you can see in the equation (3.22), the influence source component for the coefficient is S_1 because the integrations of the others over very small surface are just zero. In the plate case, however, the influence source components are S_1 and S_2 because x_3 and ξ_3 are both zero. So

$$\begin{aligned}
\int_{S_\varepsilon} \phi(\boldsymbol{\xi}) \frac{\partial (S_1 + S_2)}{\partial n_\xi} \mathrm{d}S_\varepsilon &= \int_{S_\varepsilon} \phi(\boldsymbol{\xi}) \frac{\partial}{\partial n_\xi} \left(\frac{2}{\sqrt{(\xi_1 - x_1)^2 + (\xi_2 - x_2)^2}} \right) \mathrm{d}S_\varepsilon \\
&\approx \phi(\mathbf{x}) \int_{S_\varepsilon} \frac{\partial}{\partial n_\xi} \left(\frac{2}{r} \right) \mathrm{d}S_\varepsilon; \quad r \equiv \sqrt{(\xi_1 - x_1)^2 + (\xi_2 - x_2)^2} \\
&\approx \phi(\mathrm{x})\, 2\, 2\pi \\
&= 4\pi\phi(\mathrm{x})
\end{aligned}$$

where S_ε means the very small half sphere surface that has been cut out, and $\mathbf{x}$ is on the plate surface. So (2.37) becomes

$$\begin{aligned}
-4\pi\phi(\mathbf{x}) = &\int_{S_B} \left(\phi(\boldsymbol{\xi}) \frac{\partial G(\mathbf{x};\boldsymbol{\xi})}{\partial n(\boldsymbol{\xi})} - G(\mathbf{x};\boldsymbol{\xi}) \frac{\partial \phi(\boldsymbol{\xi})}{\partial n(\boldsymbol{\xi})} \right) \mathrm{d}S_B(\boldsymbol{\xi}) \\
&+ \int_{S_\infty} \left(\phi_I(\boldsymbol{\xi}) \frac{\partial G(\mathbf{x};\boldsymbol{\xi})}{\partial n(\boldsymbol{\xi})} - G(\mathbf{x};\boldsymbol{\xi}) \frac{\partial \phi_I(\boldsymbol{\xi})}{\partial n(\boldsymbol{\xi})} \right) \mathrm{d}S_\infty(\boldsymbol{\xi}) \qquad \text{for } \mathbf{x} \text{ on } S_B
\end{aligned}$$

and (2.38) becomes

$$-4\pi\phi_I(\mathbf{x}) = \int_{S_\infty} \left(\phi_I(\boldsymbol{\xi}) \frac{\partial G(\mathbf{x};\boldsymbol{\xi})}{\partial n(\boldsymbol{\xi})} - G(\mathbf{x};\boldsymbol{\xi}) \frac{\partial \phi_I(\boldsymbol{\xi})}{\partial n(\boldsymbol{\xi})} \right) \mathrm{d}S_\infty(\boldsymbol{\xi}) \qquad \text{for } \mathbf{x} \text{ on } S_B$$

By adding above two equations, then we get

$$-4\pi\phi(\mathbf{x}) + 4\pi\phi_I(\mathbf{x}) = \int_{S_B} \left(\phi(\boldsymbol{\xi}) \frac{\partial G(\mathbf{x};\boldsymbol{\xi})}{\partial n(\boldsymbol{\xi})} - G(\mathbf{x};\boldsymbol{\xi}) \frac{\partial \phi(\boldsymbol{\xi})}{\partial n(\boldsymbol{\xi})} \right) \mathrm{d}S_B(\boldsymbol{\xi}) \qquad \text{for } \mathbf{x} \text{ on } S_B \tag{B.1}$$

From the second condition of (2.27), (B.1) becomes

$$-4\pi\phi(\mathbf{x}) + 4\pi\phi_I(\mathbf{x}) = \int_{S_B} \left(\phi(\boldsymbol{\xi}) \frac{\omega^2}{g} - i\omega u_3 \right) G(\mathbf{x};\boldsymbol{\xi})\, \mathrm{d}S_B(\boldsymbol{\xi}) \qquad \text{for } \mathbf{x} \text{ on } S_B$$

and by the Bernoulli's equation we get

$$-4\pi \frac{i}{\omega} \left(\frac{P(\mathbf{x})}{\rho_w} + g u_3 \right) + 4\pi\phi_I(\mathbf{x}) = \int_{S_B} i \frac{\omega}{\rho_w g} P(\boldsymbol{\xi}) G(\mathbf{x};\boldsymbol{\xi})\, \mathrm{d}S_B(\boldsymbol{\xi}) \tag{B.2}$$

The variational form of (B.2) is then

$$-\int_{S_B} 4\pi \frac{i}{\omega}\frac{P(\mathbf{x})}{\rho_w}\bar{P}(\mathbf{x})\,\mathrm{d}S_B(\mathbf{x}) - \int_{S_B} 4\pi \frac{i}{\omega} g u_3 \bar{P}(\mathbf{x})\,\mathrm{d}S_B(\mathbf{x}) + \int_{S_B} 4\pi\phi_I(\mathbf{x})\bar{P}(\mathbf{x})\,\mathrm{d}S_B(\mathbf{x}) = \int_{S_B}\int_{S_B} i\frac{\omega}{\rho_w g} P(\boldsymbol{\xi})G(\mathbf{x};\boldsymbol{\xi})\,\mathrm{d}S_B(\boldsymbol{\xi})\bar{P}(\mathbf{x})\,\mathrm{d}S_B(\mathbf{x}) \tag{B.3}$$

The equation for the structure, (2.50), is

$$-\int_V \omega^2\rho_s \bar{\mathbf{u}}^T\mathbf{u}\,\mathrm{d}V + \int_V \bar{\boldsymbol{\epsilon}}^T\boldsymbol{\sigma}\,\mathrm{d}V = \int_{S_B} P\,\bar{u}_3\,\mathrm{d}S_B \tag{B.4}$$

where P means the total pressure. The advantages of the above coupled equation where the total pressure and the displacements of the structure are coupled are first, we don't need to evaluate the derivative of the Green's function and second, we can get the symmetric linear system by discretization.

B.2 One dimensional beam case

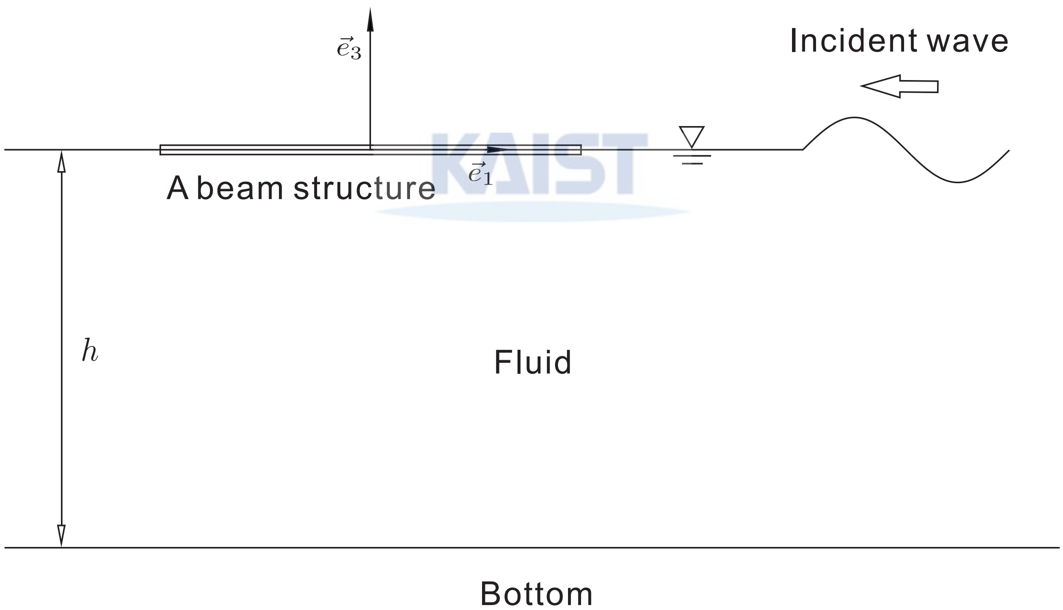

Figure B.1: Schema of one dimensional beam case

In two dimensional fluid, the free surface Green's function with strength 2π is defined by [6], [21]

$$G = \ln\sqrt{(x_1-\xi_1)^2+(x_3-\xi_3)^2} + \ln\sqrt{(x_1-\xi_1)^2+(2h+x_3+\xi_3)^2} - 2\ln h - 2\,P.V.\int_0^\infty \left[\frac{(K+k)e^{-kh}\cosh k(\xi_3+h)\cosh k(x_3+h)\cos k|x_1-\xi_1|}{k(k\sinh kh - K\cosh kh)} + \frac{e^{-kh}}{k}\right]\mathrm{d}k \tag{B.5}$$

or series representation like

$$G = -2\pi i\sum_{n=0}^{\infty}\frac{k_n^2-K^2}{k_n(k_n^2h-K^2h+K)}\cosh k_n(x_3+h)\cosh k_n(\xi_3+h)e^{ik_n|x_1-\xi_1|} \tag{B.6}$$

for finite depth case, and

$$G = \ln\sqrt{(x_1-\xi_1)^2+(x_3-\xi_3)^2} + P.V.\int_0^\infty \left[\frac{(K+k)e^{k(x_3+\xi_3)}\cos k|x_1-\xi_1|}{k(K-k)} - \frac{e^{-k}}{k}\right]\mathrm{d}k \tag{B.7}$$

for infinite depth case, where h is the water depth, $K=\frac{\omega^2}{g}$, k_0 is the positive real root of the dispersion relation, and k_1, k_2, ... are the positive pure imaginary roots of the dispersion relation multiplied by $-i$. (2.35) becomes

$$\int_{S_C}\left(\phi(\boldsymbol{\xi})\frac{\partial G(\mathbf{x};\boldsymbol{\xi})}{\partial n(\boldsymbol{\xi})} - G(\mathbf{x};\boldsymbol{\xi})\frac{\partial\phi(\boldsymbol{\xi})}{\partial n(\boldsymbol{\xi})}\right)\mathrm{d}S_C(\boldsymbol{\xi}) = \begin{cases} 0 & \text{for } \mathbf{x} \text{ outside } S_C \\ \pi\phi(\mathbf{x}) & \text{for } \mathbf{x} \text{ on } S_C \\ 2\pi\phi(\mathbf{x}) & \text{for } \mathbf{x} \text{ inside } S_C \end{cases} \tag{B.8}$$

With above equations, we can obtain

$$\pi\phi(\mathbf{x}) - 2\pi\phi_I(\mathbf{x}) = \int_{S_B}\left(\phi(\boldsymbol{\xi})\frac{\partial G(\mathbf{x};\boldsymbol{\xi})}{\partial n(\boldsymbol{\xi})} - G(\mathbf{x};\boldsymbol{\xi})\frac{\partial\phi(\boldsymbol{\xi})}{\partial n(\boldsymbol{\xi})}\right)\mathrm{d}S_B(\boldsymbol{\xi}) \qquad \text{for } \mathbf{x} \text{ on } S_B \tag{B.9}$$

So, the variational forms of the coupled equations for two dimensional case are

$$-\int_V \omega^2\rho_s\bar{\mathbf{u}}^T\mathbf{u}\,\mathrm{d}V + \int_V \bar{\boldsymbol{\epsilon}}^T\boldsymbol{\sigma}\,\mathrm{d}V = -\int_{S_B} i\omega\rho_w\phi\bar{\mathbf{u}}^T\mathbf{n}\,\mathrm{d}S_B - \int_{S_B}\rho_w g u_3\bar{\mathbf{u}}^T\mathbf{n}\,dS_B \tag{B.10}$$

and

$$\begin{aligned}\int_{S_B}\pi\phi(\mathbf{x})\bar{\phi}(\mathbf{x})\,\mathrm{d}S_B(\mathbf{x}) - \int_{S_B}2\pi\phi_I(\mathbf{x})\bar{\phi}(\mathbf{x})\,\mathrm{d}S_B(\mathbf{x}) = \\ \int_{S_B}\int_{S_B}\left(\phi(\boldsymbol{\xi})\frac{\partial G(\mathbf{x};\boldsymbol{\xi})}{\partial n(\boldsymbol{\xi})} - i\omega G(\mathbf{x};\boldsymbol{\xi})\mathbf{u}(\boldsymbol{\xi})\cdot\mathbf{n}(\boldsymbol{\xi})\right)\mathrm{d}S_B(\boldsymbol{\xi})\bar{\phi}(\mathbf{x})\,\mathrm{d}S_B(\mathbf{x})\end{aligned} \tag{B.11}$$

In the beam case where S_B is at $x_3=0$, above coupled equations with same procedure in the plate case could be changed like

$$-\int_V \omega^2\rho_s\bar{\mathbf{u}}^T\mathbf{u}\,\mathrm{d}V + \int_V \bar{\boldsymbol{\epsilon}}^T\boldsymbol{\sigma}\,\mathrm{d}V = \int_{S_B} P\,\bar{u}_3\,\mathrm{d}S_B \tag{B.12}$$

and

$$\begin{aligned}\int_{S_B}2\pi\frac{i}{\omega}\frac{P(\mathbf{x})}{\rho_w}\bar{P}(\mathbf{x})\,\mathrm{d}S_B(\mathbf{x}) + \int_{S_B}2\pi\frac{i}{\omega}gu_3\bar{P}(\mathbf{x})\,\mathrm{d}S_B(\mathbf{x}) - \int_{S_B}2\pi\phi_I(\mathbf{x})\bar{P}(\mathbf{x})\,\mathrm{d}S_B(\mathbf{x}) = \\ \int_{S_B}\int_{S_B} i\frac{\omega}{\rho_w g}P(\boldsymbol{\xi})G(\mathbf{x};\boldsymbol{\xi})\,\mathrm{d}S_B(\boldsymbol{\xi})\bar{P}(\mathbf{x})\,\mathrm{d}S_B(\mathbf{x})\end{aligned} \tag{B.13}$$

The same advantages of the plate case could be applied to the one dimensional beam case with above equations.

References

[1] Abramowitz M. and Stegun I.A., *Handbook of Mathematical Functions with Formulas, Garphs, and Mathematical Tables*, Government Printing Office, Washington, and Dover, New York, 1964.

[2] Bathe K. J. and Dvorkin E. N., A Formulation of General Shell Elements–The Use of Mixed Interpolation of Tensorial Components, *Engineering Computations*, Vol. 3, pp. 178-191, 1986.

[3] Bathe K. J., *Finite element procedures*, Prentice Hall, 1996.

[4] Bishop R.E.D. and Price W.G., *Hydroelasticity of Ships*, Cambridge University Press, Cambridge, 1979.

[5] Chapelle D. and Bathe K. J., *The finite element analysis of shells - Fundamentals*, Springer, 2003.

[6] John F., On the motion of floating bodies II, *Communications on Pure and Applied Mathematics*, Vol.3, pp.45-101, 1950.

[7] Kashiwagi M., Research on hydroelastic responses of VLFS: recent progress and future work, *International Journal of Offshore and Polar Engineering*, Vol. 10, iss. 2, pp. 81-90, 1998.

[8] Khabakhpasheva T.I. and Korobkin, A.A., Hydroelastic behaviour of compound floating plate in waves, *Journal of engineering mathematics*, Vol. 44, pp. 21-40, 2002.

[9] Newman J. N., *Marine Hydrodynamics*, The MIT Press, 1977.

[10] Newman J. N., An expansion of the oscillatory source potential, *Applied Ocean Research*, Vol.6, pp.116-117, 1984.

[11] Newman J.N., Approximations for the Bessel and Struve functions, *Mathematics of Computation*, Vol.43, pp.551-556, 1984.

[12] Newman J.N., Double-precision evaluation of the oscillatory source potential, *Journal of Ship Research*, Vol.28, pp.151-154, 1984.

[13] Newman J. N., Algorithms for the free-surface Green function, *Journal of Engineering Mathematics*, Vol. 19, pp. 57-67, 1985

[14] Noblesse F., The Green function in the theory of radiation and diffraction of regular water waves by a body, *Journal of Engineering Mathematics*, Vol.16, pp.137-169, 1982.

[15] Riggs H.R., Niimi K.M., and Huang L.L., Two benchmark problems for three-dimensional, linear hydroelasticity, *Journal of Offshore Mechanics and Arctic Engineering*, Vol. 129, iss. 3, pp. 149-157, 2007.

[16] Saad Y. and Schultz M. H., GMRES: A Generalized Minimal Residual Algorithm for Solving Nonsymmetric Linear Systems, *Society for Industrial and Applied Mathematics*, Vol. 7, pp. 856-869, 1986.

[17] Saad Y. A flexible inner-outer preconditioned GMRES algorithm, *Society for Industrial and Applied Mathematics*, Vol. 14, iss. 2, pp. 461-469, 1993.

[18] Taylor R.E., Hydroelastic analysis of plates and some approximations, *Journal of engineering mathematics*, Vol. 58, pp. 267-278, 2007.

[19] WAMIT, *User's Manual*, WAMIC Inc.

[20] Watanabe E., Utsunomiya T. and Wang C.M., Hydroelastic analysis of pontoon-type VLFS: a literature survey, *Engineering Structures*, Vol. 26, iss. 2, pp. 245-256, 2004.

[21] Wehausen J. V. and Laitone E. V., Surface waves, *Encyclopedia of Physics*, Vol. 9, pp. 446-778, Springer-Verlag, 1960.

[22] Yago K. and Endo H., On the hydroelastic response of box-shaped floating structure with shallow draft, *Journal of the Society of Naval Architects of Japan*, Vol. 182, pp. 307-317, 1997

Summary

Hydroelastic analysis of three dimensional floating structures

거대한 해양 구조물의 해양파에 대한 거동은 기존의 강체 해석법이 아닌 해양 구조물의 유탄성 효과를 고려한 해석법이 요구된다. 이에 대한 연구들이 활발히 진행되어 왔으나 해양 구조물의 모델링에 있어서 판이나 보에 국한 되어 왔다. 우리는 보다 발전된 해양 구조물의 유탄성 해석을 위하여 해양 구조물을 쉘 구조물로 모델링하여 그 거동을 살펴보고자 한다. 이를 위하여 먼저 3차원 해양 구조물의 유탄성 해석에 관한 수학적 모델을 제시한다. 그런 다음 3가지 실험 모델을 토대로 수학적 모델의 결과를 도출하며 실험 모델의 결과 및 상용 유탄성 해석 툴의 결과와 비교를 해 본다.